ISTANBUL TECHNICAL UNIVERSITY ★ GRADUATE SCHOOL OF SCIENCE ENGINEERING AND TECHNOLOGY

ELECTROSPUN NANOFIBERS OF ONE STEP SYNTHESIZED POLY(ACRYLONITRILE-CO-VINYL ACETATE)/ POLYPYRROLE COMPOSITES

M.Sc. THESIS

Burcu ARMAN

Department of Polymer Science and Technology

Polymer Science and Technology Programme

JUNE 2012

ISTANBUL TECHNICAL UNIVERSITY ★ GRADUATE SCHOOL OF SCIENCE ENGINEERING AND TECHNOLOGY

ELECTROSPUN NANOFIBERS OF ONE STEP SYNTHESIZED POLY(ACRYLONITRILE-CO-VINYL ACETATE)/ POLYPYRROLE COMPOSITES

M.Sc. THESIS

Burcu ARMAN

(515101002)

Department of Polymer Science and Technology

Polymer Science and Technology Programme

Thesis Advisor: Prof. Dr. A. Sezai SARAÇ

JUNE 2012

İSTANBUL TEKNİK ÜNİVERSİTESİ ★ FEN BİLİMLERİ ENSTİTÜSÜ

TEK ADIMDA SENTEZLENEN POLİ(AKRİLONİTRİL-KO-VİNİL ASETAT)/ POLİPİROL KOMPOZİTLERİNDEN ELEKTROÇEKİM YÖNTEMİ İLE NANOLİF ELDESİ

YÜKSEK LİSANS TEZİ

Burcu ARMAN
(515101002)

Polimer Bilim ve Teknolojileri

Polimer Bilim ve Teknolojileri Programı

Tez Danışmanı: Prof. Dr. A. Sezai SARAÇ

HAZİRAN 2012

Burcu Arman, a **M.Sc.** student of ITU **Graduate School of Science, Technology andEngineering** student ID **515101002**, successfully defended the **thesis/dissertation** entitled **ELECTROSPUN NANOFIBERS OF ONE STEP SYNTHESIZED POLY(ACRYLONITRILE-CO-VINYL ACETATE)/ POLYPYRROLE COMPOSITES"** which he/she prepared after fulfilling the requirements specified in the associated legislations, before the jury whose signatures are below.

Thesis Advisor:	**Prof. Dr. A. Sezai SARAÇ** Istanbul Technical University	.....
Jury Members	**: Prof.Dr. Hulusi ÖZKUL** Istanbul Technical University	.....
	Prof. Dr. Hale KARAKAŞ Istanbul Technical University	.....

Date of Submission : 4 May 2012

Date of Defense : 7 June 2012

To my family,

FOREWORD

I would like to express my gratitude to my thesis supervisor, Prof. Dr. A.Sezai SARAÇ for his continuous encouragement, guidance, helpful critics and discussions in my studies.

I would like to thank İlhan KOŞAN from Aksa Acrylic Chemistry Company for encouragement throughout this research.

I would like to give my special thanks to my laboratory friends; Selda ŞEN, Suat ÇETİNER, Derya ÇETECİOĞLU, Merih Zeynep AVCI, Başak DEMİRCİOĞLU, Timuçin BALKAN, Ece POLAT, Nazif Uğur KAYA, Aslı GENÇTÜRK, Yasemin YERLİKAYA, Fatma Gül GÜLER, Keziban HÜNER, Didem GİRAY, Ezgi İŞMAR, Mehmet Giray ERSÖZOĞLU and Hacer DOLAŞ for their collaborative and friendly manner. I would like thanks to my collegue, Mustafa Edhem KAHRAMAN from Istanbul Technical University TEMAG laboratory.

I would like to thank to Sevilay KOÇ ÖZKUL and teeny ILGAZ ÖZKUL for their positive energy, Sümeyye ÖZER for her full support, Muzaffer KUZUBAŞOĞLU for his help, understanding and also full support.

Most of all, I would like to thanks my family, especially my mother Meryem ARMAN, my father Serdar ARMAN, my brother Ali Arda ARMAN, my aunt Gülay İŞİSAĞLAM and my cousin Ecem İŞİSAĞLAM. For all those times they stood by me and heartedly supported. I was able to accomplish everything in my life thanks to their eternal love.

Finally, I would like to thank all of my other friends for all their emotional assists and motivation during this extremely difficult accomplishment.

June 2012

Burcu ARMAN

Textile Engineer

TABLE OF CONTENTS

Page

FOREWORD ..... **ix**
TABLE OF CONTENTS ..... **xi**
ABBREVIATIONS ..... **xiii**
LIST OF TABLES ..... **xv**
LIST OF FIGURES ..... **xvii**
SUMMARY ..... **xix**
ÖZET ..... **xxi**
1. INTRODUCTION **1**
2. THEORETICAL PART **3**
2.1 Acrylonitrile, Polyacrylonitrile and Poly(acrylonitrile-co-vinyl acetate) 3
2.2 Emulsion Polymerization 5
2.3 Free Radical Polymerization 7
2.3.1 Chain Initiation 7
2.3.2 Chain Propagation 8
2.3.3 Chain Termination 8
2.4 Conductive Polymers 9
2.4.1 Synthesis of Polypyrrole 10
Chemical Polymerization 10
Counterion-Induced Solubilization 11
Colloidal PPy Dispersions 11
2.4.2 Properties of Polypyrrole 12
2.4.3 Application areas of conductive polymers 14
2.5 Nanofiber 15
2.6 Electrospinning 16
2.6.1 Electrospinning process 17
2.6.2 Effects of parameters on electrospinning 19
2.6.3 Solution parameters 19
2.6.4 Processing parameters 21
3. EXPERIMENTAL PART **25**
3.1 Materials 25
3.2 Synthesis of P(AN-co-VAc) Copolymer 25
3.3 Coating of P(AN-co-VAc) Latex Particles with Polypyrrole 26
3.4 Preparation of Electrospinning Solutions 28
3.5 Electrospinning Process Setup 29
3.6 Characterization of P(AN-co-VAc) Copolymer and P(AN-co-VAc)/PPy Composites 29
4. RESULTS AND DISCUSSION **33**
4.1 Copolymer and Composite Characterization 33
4.1.1 FTIR-ATR spectrophotometric analysis 33
4.1.2 Nuclear magnetic resonance (NMR) spectroscopy of P(AN-co-VAc) and P(AN-co-VAc)/PPy 36
4.1.3 UV- Visible spectrophotometric analyses 38
4.1.4 Differential scanning calorimetry measurement (DSC) of P(AN-co-VAc) and P(AN-co-VAc)/PPy composites 39

4.1.5 T_g Determination by DMA 40
4.1.6 Viscosity and molecular weight determination 42
4.1.7 Particle size measurements, SEM 43
4.1.8 Dynamic mechanical analysis of composites 45
4.1.9 Impedance spectroscopy measurements 46
4.2 Morhology of Fibers 47
5. CONCLUSION 51
REFERENCES 53
CURRICULUM VITAE 63

ABBREVIATIONS

AFM	**:** Atomic Force Microscopy
AN	**:** Acrylonitrile
APS	**:** Ammonium persulfate
DMA	**:** Dynamic Mechanical Analyser
DMF	**:** Dimethylformamide
DBSA	**:** Sodium Dodecyl Benzene Sulfonic acid
DSC	**:** Differential Scanning Calorimetry
FTIR-ATR	**:** Fourier Transform Infrared Spectroscopy
M_v	**:** Viscosity Average Molecular Weight
NMR	**:** Nucleear Magmetic Resonance
PAN	**:** Polyacrylonitrile
P(AN-co-VAc)	**:** Poly(Acrylonitrile-co-Vinyl acetate)
P(AN-c0-VAc)@PPy$_{1\text{-}2\text{-}3\text{-}4}$	**:** Composites in different Py feed mole fraction: 0.030%, 0.045%, 0.060%, 0.075%
PPy	**:** Polypyrrole
PVAc	**:** Poly(vinyl acetate)
SEM	**:** Scanning Electron Microscopy
T_g	**:** Glass Transition Temperature
η	**:** Intrinsic Viscosity
η_s	**:** Specific Viscosity
UV-Vis	**:** Ultraviole Visible

LIST OF TABLES

Page

Table 2.1: Typical free radical chain copolymerization reactivity ratios at 60°C [28]. 4

Table 3.1: Feed content of Py and content of PPy in composition. 27

Table 3.2: Electrospinning parameters for various composites. 28

Table 4.1: P(AN-co-VAc), P(AN-co-VAc)/PPy specific viscosity results. 42

Table 4.2: Toughness of polymers were shown in the table. 45

Table 4.3: Standart deviation values and average nanofiber diameters. 49

LIST OF FIGURES

Page

Figure 2.1: General formula of acrylonitrile. 3
Figure 2.2: Schematic view of emulsion polymerization [39]. 6
Figure 2.3: DBSA. 11
Figure 2.4: Electronic energy diagrams for (a) neutral PPy, (b) polaron, (c) bipolaron, and (d) fully doped PPy. 12
Figure 2.5: Electronic structures of (a) neutral PPy, (b) polaron in partially doped PPy and (c) bipolaron in fully doped PPy [78]. 13
Figure 2.6: Overview of some application areas of conducting polymers. 15
Figure 2.7: SEM image of nanofibers from previous studies[160] 16
Figure 2.8: Typical setup of electrospinning device [103]. 18
Figure 3.1: Monomers used in synthesis of P(AN-co-VAc). 25
Figure 3.2: P(AN-co-VAc) structure. 26
Figure 3.3: Experimental setup for synthesis of P(AN-co-VAc). 26
Figure 3.4: Latex form of P(AN-co-VAc), P(AN-co-VAc)@PPy1, P(AN-co-VAc)@PPy2, P(AN-co-VAc)@PPy3, P(AN-co-VAc)@PPy4, respectively. 27
Figure 3.5: The structure of composite. 27
Figure 3.6: View of electrospinning solutions of (a) P(AN-co-VAc) and (b) P(AN-co-VAc)@ PPy_4. 28
Figure 3.7: A representative view of electrospinning devices. 29
Figure 3.8: Perkin Elmer FTIR-ATR spectrophotometer. 30
Figure 3.9: Agilent VNMRS 500 MHz Nuclear Magnetic Resonance Spectrometer. 30
Figure 3.10: TA Q1000 DSC instrument. 31
Figure 3.11: Nanosurf EasyScan2 AFM. 31
Figure 3.12: TA Q800 Dynamic Mechanical Analyser. 32
Figure 3.13: Perkin Elmer UV Visible Spectrophotometer. 32
Figure 3.14: Parstat 2263 Electrochemical Analyser. 32
Figure 4.1: FTIR-ATR spectra of powder form of P(AN-co-VAc). 33
Figure 4.2: FTIR-ATR spectra of prepared P(AN-co-VAc) nanofibers (red line), and P(AN-co-VAc) in powder form (black line). 34
Figure 4.3: FTIR-ATR spectra of P(AN-co-VAc) copolymer and composites of P(AN-co-VAc)/PPy. 35
Figure 4.4: FTIR-ATR spectra of P(AN-co-VAc) copolymer and composites of P(AN-co-VAc)/PPy4, Py feeding ratio of 0.075 mole %. 36
Figure 4.5: NMR spectrum of P(AN-co-VAc). 37
Figure 4.6: NMR Spectrum of P(AN-co-VAc)@PPy_4 37
Figure 4.7: UV-Vis Spectrum of P(AN-co-VAc)@PPy_1, P(AN-co-VAc)@PPy_2, P(AN-co-VAc)@PPy_3, P(AN-co-VAc)@PPy_4. 38
Figure 4.8: Dissolved nanofibers of P(AN-co-VAc), P(AN-co-VAc)@PPy_1, P(AN-co-VAc)@PPy_2, P(AN-co-VAc)@PPy_3, P(AN-co-VAc)@PPy_4. 38
Figure 4.9: Correlation between FTIR-ATR absorbance ratio of CN str. ($1451cm^{-1}$)/[CN str. ($1451cm^{-1}$)/ C-O-C str. ($1232cm^{-1}$)], UV-Vis absorbance values at 430 nm and Py feed mole fraction. 39

Figure 4.10: DSC graph of P(AN-co-VAc), P(AN-co-VAc)@PPy_1, P(AN-co-VAc)PPy_4. 40
Figure 4.11: T_g values of composites obtained by DMA. 41
Figure 4.12: Correlation between Tg values obtained from DSC and DMA corresponding to Py feed mole fraction (mole %). 41
Figure 4.13: The intrinsic viscosity calibration curve (η_s/C versus C). 42
Figure 4.14: SEM images of latex particles of copolymer (a) and composites including different pyrrole content (b), (c), (d), (e). 44
Figure 4.15 : Relation between Py content and size of latex particles in composites. 45
Figure 4.16: Stress-strain curve of polymers that were obtained by DMA. 46
Figure 4.17: Admittance diagrams of P(AN-co-VAc)@PPy_{1-2-3} solution in DMF and P(AN-co-VAc) in DMF solution. 47
Figure 4.18: SEM images of P(AN-co-VAc)(a) and the samples at different PPy content: P(AN-co-VAc)@PPy_1, 0.030 mole % (b), P(AN-co-VAc)@PPy_2 , 0.045 mole % (c), P(AN-co-VAc)@PPy_3 , 0.060 mole % (d) and P(AN-co-VAc)@PPy_4 , 0.075 mole % (e)..... 48
Figure 4.19: Photos of obtained nanofiber webs..... 49
Figure 4.20: Relationship between nanofiber diameter, specific viscosity and Py feed mole fraction, %. 49
Figure 4.21: SEM and AFM images of P(AN-co-VAc) (a) and P(AN-co-VAc)@PPy_4 (b)..... 50

ELECTROSPUN NANOFIBERS OF ONE STEP SYNTHESIZED POLY(ACRYLONITRILE-CO-VINYL ACETATE)/ POLYPYRROLE COMPOSITES

SUMMARY

In the first part of this study, synthesis of Poly(Acrylonitrile-co-vinyl acetate)/Polypyrrole composite particles with uniform size and morphology was objected using one step polymerization technique that involves swelling and coating of polypyrrole(PPy) into P(AN-co-VAc) latex particles. As an initial, free radical copolymerization of acrylonitrile (AN)-vinyl acetate (VAc) was synthesized by emulsion polymerization method using ammonium persulfate (APS) and Sodium dodecylbenzenesulfonic acid (DBSA). P(AN-co-VAc)/PPy composites were synthesized by adding the pyrrole monomers into the continued reaction. Composites were obtained with continued polymerization during 18 hours with adding different quantity of pyrrole in 4 sample flasks and stirring and mixing during the reaction time. Composites were characterized in terms of chemical composition, surface morphology, particle size, conductivity, thermal and mechanical properties by using NMR, Fourier Transform Infrared - Attenuated Total Reflectance spectrophotometer(FTIR-ATR), Scanning Electron Microscope(SEM), Parstat Electrochemical Analyser via EIS measurement, UV-Visible Spectrophotometer, Differential Scanning Calorimeter(DSC) and Dynamic Mechanical Analyser, DMA. FTIR-ATR spectra and NMR spectrum of copolymer revealed that AN and VAc had participated in polymerization effectively and also FTIR-ATR, UV-Vis spectra and especially NMR spectrum of P(AN-co-VAc)/PPy composites clearly observed that Py had participated in polymerization. The morphology of latex particles were indicated by SEM images. Participation of PPy to the copolymer latex particles were obviously obtained. The thermal effect of PPy on the copolymer structure was investigated by DSC and DMA analysers. Increase in glass transition temperatures with increasing feed pyrrole ratio were in spite of the lack of chain flexibility of polymer. Moreover, DMA also showed that the brittleness of PPy lead to decrease in tensile strength of polymeric films.

The second aim of the study was in order to obtain nanofibers from the P(AN-co-VAc) copolymer and P(AN-co-VAc)/PPy composites by the electrospinning method. Moreover, the relationship between Py content, viscosity and fiber diameters were investigated and it was investigated that increase in initially feed ratio of Py content lead to decrasing nanofiber diameter was determined. Morphological properties of nanofibers were examined by scanning electron microscopy (SEM) and atomic force spectroscopy (AFM). If we make comparison between nanofiber diameters of P(AN-co-VAc) copolymer and P(AN-co-VAc)/PPy composites, it was clearly seen that nanofiber diameters were strongly dependent on pyrrole content in composites. Because of the the improvement in PPy solubility with the effect of dodecyl benzene

sulfonic acid (DBSA), smoother and more homogeneus fiber morphology were obtained. Mole percent of the initially added Py concentration varies from 0.030% to 0.075%, the average diameters of the nanofibers were reduced from 200 to 120 nm. It is observed that the diameters of the fibers decrease slightly with the increase of Py feed ratio in composition with the increase of the initially added Py concentrations, some beads begin to appear. It can be said that this is result of the increased PPy content in the electrospinning solutions and also decrease in viscosity.

TEK ADIMDA SENTEZLENEN POLİ (AKRİLONİTRİL-KO-VİNİL ASETAT)/ POLİPİROL KOMPOZİTLERİNDEN ELEKTROÇEKİM YÖNTEMİ İLE NANOLİF ELDESİ

ÖZET

Bu çalışma iki bölümden oluşmaktadır. Birinci bölümde, hedeflenen amaç Poli (Akrilonitril-ko-Vinil asetat)/Polipirol kompozitleri oluşturmaktır. Bu amaca yönelik yapılan ilk çalışma matris olarak seçilen Poli(Akrilonitril-ko-Vinil asetat) kopolimeri sentezlemektir. Ağırlıkça % 70 akrilonitril monomeri ve % 30 vinil asetat monomeri sisteme beslenmiştir. P(AN-co-VAc) kopolimerini oluşturmak için polimerizasyon tekniği olarak emülsiyon polimerizasyonu yöntemi kullanılmıştır. Emülsiyon polimerizasyosunda birbirine karışmayan iki faz bulunmaktadır. Monomer fazı dağıtma fazı içinde homojen olarak dağılır. Emülsiyon yapıcı maddeler kullanılarak monomer fazı dağıtma fazı içerisinde tek düze küresel partiküller homojen halde bulunur. Polimerizasyonda başlatıcı olarak Amonyum persülfat kullanılmıştır. Emülsiyon yapıcı madde olarak ise çok kullanılan yüzey aktif maddelerden biri olan dodesil benzen sülfonik asit tuzu kullanılmıştır. P(AN-co-VAc) kopolimerini sentezlemek için gereken reaksiyon süresi 3 saat ve reaksiyon sıcaklığı 70^{o}C'dir. Üç saat sonunda elde edilen lateks halde bulunan P(AN-co-VAc) oda sıcaklığına getirildikten sonra 4 eşit hacme ayrılmıştır. Lateks halde bulunan P(AN-co-VAc) kopolimerininin bir kısmına pirol eklenmemiş ve karşılaştırma amacıyla kullanılmıştır. Ayrılan numunelere farklı miktarlarda pirol monomeri eklenmiştir. Pirol monomeri eklendikten sonra 18 saat boyunca oda sıcaklığında karıştırılmıştır. Artan başlatıcı polipirol sentezinde polimerizasyonun gerçekleşmesinde kullanışmıştır. Böylece P(AN-co-VAc) partiküllerine polipirol kaplama işlemi gerçekleştirilmiştir. Tek adımda kompozit oluşturulmuştur. Her bir numune için oluşturulan partiküllerin bir kısmı Taramalı elektron mikroskobuyla morfoloji ve boyut tayini için lateks halde ayrılmıştır. Kalan kısım ise yine her bir numune için ilk önce metanolde çöktürülmüş, daha sonra süzme işlemi ile ethanol ve saf sudan geçirilmiştir.

Elde edilen kompozitlerin yapısını incelemek amacıyla FTIR-ATR, UV-Vis, NMR analizi yapılmıştır. Termal, morfolojik ve iletkenlik özelliklerini incelemek amacıyla ise DSC, DMA, SEM, PARSTAT cihazları kullanılmıştır. FTIR-ATR spektrometresi ile yapılan analizler sonucunda akrilonitril (AN) ve vinil asetat (VAc) monomerlerinin polimerleşerek yapıya girdiği gözlemlenmiştir. UV Görünür bölge spektrofotometresi ile de yapıda polipirol bulunduğu saptanmıştır. Polipirolün birimlerine ait π-π^* geçisleri nedeniyle absorpsiyon pikleri elde edilmiştir. Değişen pirol(PPy) miktarlarına göre spektrumdaki piklerde değişimler ortaya konmuştur. Nükleer magnetik rezonans spektrumu (NMR) ölçümleri 250 MHz Bruker AC Aspect 3000 NMR ve 500 MHz Agilent VNMRS Nuclear Magnetic Resonance

spektrometre cihazları kullanılarak yapılmıştır. NMR analizlerinden elde edilen verilerde aynı şekilde AN, VAc ve PPy yapıda bulunduğu gözlemlenmiştir. δ=2.07 ppm'de akrilonitril ve vinil asetat $–CH_2$ protonuna ait pik, δ=3.12 ppm'de akrilonitril –CH protonuna ait pik, δ=5.13 ppm'devinil asetat –CH protonuna ait pik, δ=8 ppm'de ise polipirol halkalarına ait pik oluşumu saptanmıştır. Dinamik mekanik analiz (DMA) cihazı ile polimerlerin mekanik özellikleri incelenmiştir. DMA cihazı ile ölçüm yapabilmek için her bir polimerden ince filmler hazırlanmıştır. Bu filmler cihaza uygun boyutlarda kesilerek ölçüm için hazır hale getirilmiştir. Çekme gerilmesine karşılık uzama grafiğinden filmlerin elastik modülleri hesaplanmıştır. Yapıya eklenen pirol miktarı arttıkça elastik modül değerlerinde düşüş gözlemlenmiştir. Bu da yapıdaki pirol miktarının artmasıyla filmlerin çekme mukavemetlerinde düşüş olduğunu göstermiştir. DMA cihazı ile yapılan diğer bir analiz ise frekansa bağlı sıcaklık artışına dayanan testler yapılmıştır. Numunelerin termal özellikleri hakkında veriler elde edilmiştir. Bu testlerden elde edilen verilerde malzemelerin camsı geçiş sıcaklıkları tespit edilmiştir. Yapıya giren polipirol miktarı arttıkça camsı geçiş sıcaklıklarında bir artış gözlemlenmiştir. Bunun sebebi ise polipirol katılımının zincir esnekliğini düşürmesinden dolayıdır. Termal özellikler diferansiyel taramalı kalorimetri (DSC) ile de incelenmiştir. DSC ile yapılan analiz ile de yine yapıya giren polipirol miktarının artışına bağlı olarak camsı geçiş sıcaklıklarında da artış gözlemlenmiştir. Bu yapıya giren polipirol polimerinin zincir esnekliğini düşürmesinden kaynaklanmaktadır. Emülsiyon polimerizasyonu sonucunda latex halde bulunan nanopartiküllerin morfolojik özelliklerini incelemek amacıyla taramalı elektron mikroskobu cihazı kullanılmıştır. Bu analiz ile içerisinde polipirol bulundurmayan latex partiküllerinin ortamda homojen olarak dağılımı söz konusudur. Yapıya giren polipirol miktarı artmasıyla partiküllerin morfolojilerinde değişiklikler ortaya çıkmıştır. İlk olarak en az miktarda polipirol içeren numunedeki partikül boyutu incelendiğinde çapta incelme tespit edilmiştir. Bu lateks halde akrilonitril vinil asetat kopolimerinin pirol damlatarak bir 18 saat daha karıştırılması sebebiyledir. Eklenen pirol miktarı arttıkça çapta bir artış gözlemlenmiştir. Ayrıca SEM görüntülerinden elde edilen sonuçlar göstermektedir ki polipirol partiküllerin çevresine ve kısmen içine girmiş şekilde görülmektedir. Ubbelohde viskozimetresi kullanılarak çözücü olarak DMF kullanılarak 28 ^oC'de ağırlıkça % 30 VAc içeren P(AN-ko-VAc) kopolimerinin intrinsik viskozitesi ölçülmüştür. P(AN-co-VAc) kopolimerinin moleküler ağırlığı figure 4.13'teki grafikte yer alan kesişim değeri Mark-Houwink denklemlerinde yerine konularak hesaplanmıştır. Bu hesaba gore kopolimerin moleküler ağırlığı 380,190 g/mol olarak bulunmuştur. Bunun yanında P(AN-ko-VAc) kopolimer ve P(AN-ko-VAc)/PPy kompozitlerinin özgül viskoziteleri yine 28 ^oC'de Ubbelohde viskozimetre kullanılarak hesaplanmıştır. Elde edilen veriler eklenen pirol miktarı arttıkça özgül viskozitenin düştüğünü göstermiştir. Literatürde iletken polimerlerin moleküler ağırlıklarının düşük olduğu belirtildiğinden; PPy içeren kompozitlerin özgül viskozitelerde düşüş gözlemlenmesi bununla ilişkilendirilebilir.

Çalışmanın ikinci bölümünde ise amaç elde edilen Akrilonitril/Vinil asetat kopolimeri ve Poli(Akrilonitril-ko-Vinil asetat)/Polipirol kompozitleri ile nanolifler oluşturmaktır. Bu çalışmada izlenen yöntem; her bir numuneler için elektroçekim cihazı kullanılarak nanolifler elde etmektir. Oluşturulan nanoliflerin morfolojik özellikleri taramalı elektron mikroskobu (SEM) ve atomic güç mikroskobu (AFM) ile incelenmiştir. Nanofiber oluşturmak için polimerlerin ağırlıkça % 10'u DMF

içerisinde çözülerek hazırlanan çözeltiden nanolif eldesi oluşturulmuştur. Elektroçekim parametreleri ve çözelti konsantrasyonu her numune için aynı şekilde tutulmuştur. Başlangıçta eklenen pirol miktarı göz önünde tutularak oluşan nanofiberlerin çapları ve morfolojileri incelenmiştir. Eklenen pirol miktarının arttışına karşılık nanofiber çaplarında azalış gözlemlenmiştir. Başlangıçta eklenen pirol miktarı molce %0.030 ile %0.075 aralığında değişirken nanofiber çapları da bununla orantılı olarak 200 nm- 120 nm aralığında azalmıştır. Ayrıca yapıdaki polipirol miktarı arttıkça nanofiberler üzerinde boncuklu yapıların oluştuğu ortaya çıkmıştır. Başlangıçta eklenen pirol miktarı, çözeltilerin viskoziteleri ve nanolif çapları arasındaki ilişki incelenmiştir. Kompozitlerdeki pirol miktarı arttıkça nanolif çapında düşüş gözlemlenmiştir. Nanofiberlerin morfolojik özellikleri taramalı elektron mikroskobu (SEM) ve atomik güç mikroskobu (AFM) ile incelenmiştir. Nanofiber çaplarında gözlenen azalma, malzemelerin viskozitelerindeki düşüşle doğru orantılıdır ve aynı trendi göstermektedir. Elde edilen nanofiberlerin iletkenlik özelliklerini incelemek amacıyla nanofiberler tekrar DMF çözücüsü ile çözülmüştür. Bu çözeltilerin PARSTAT cihazı kullanılarak yapılan empedans (EIS) ölçümlerinden faydalanarak iletkenlikleri incelenmiştir. Çözelti halinde ölçüm gerçekleştirilmiştir. Admitans grafiklerinden elde edilen verilerle iletkenlikleri saptanmıştır. Admittance grafiğinden elde edilen veriler Y=1/Z formülünde yerine konularak çözelti halindeki malzemelerin iletkenlikleri hesaplanmıştır. Yapıya giren polipirol miktarı arttıkça iletkenlik özelliklerinde de artış gözlemlenmiştir. Yapıda bulunan polipirol miktarı arttıkça buna bağımlı diğer özellikler karşılaştırıldığında nanofiber çapında gözlenen düşüşe karşılık iletkenlik özelliklerinde artış ve özgül viskozitelerinde düşüş saptanmıştır.

Yapılan çalışma sonucunda elde edilen nanofiberler membran olarak çözeltiden metal iyonlarının (Au, Ag, vb.) geri dönüşümünde kullanılabilme özelliğinde olduğundan ilerleyen çalışmalarda bu amaçla uygulanabilir. İletkenlik özelliklerine bağlı olarak akıllı tekstiller, güneş pilleri, sensörler gibi uygulama alanlarında kullanılabilme durumu söz konusudur.

1. INTRODUCTION

Conducting polymers like polyaniline, polythiophene, polyacetylene, poly (p-phenylene sulfide) and poly (p-phenylene vinylene), polypyrrole etc. have been extensively studied in recent time because of their good conductivity [1] and their potential applications in various fields like sensors [2–4], actuators [5,6], catalysis[7], field effect transistors[8], light emitting diodes[9], capacitors[10] etc. But they are often brittle in nature and hence very difficult to make film from them. In order to improve the process difficulty much attention has been made in combining these conducting polymers with mechanically stable insulating polymers to give core–shell morphology. These composite particles have manifold applications such as antistatic coating, dampers, clutches, electrodes, separation membranes, electro chromic devices, electrochemomechanical actuators, and sensors[11,12]. These core–shell conducting composites have two advantages. Firstly, depending on the type of insulating polymer used as core these conducting polymer-coated latex particles can exhibit very good mechanical stability and secondly the amount of conducting polymer used can be greatly reduced in the shell phase without much loss of conductivity [13].

Polypyrrole (PPy) is one of the most promising conducting polymers due to its high electrical conductivity and good chemical stability, but its conjugated structure limits the processability, flexibility, and strength. These limitations can be overcome by making composites [14-17].

Nanofibers produced by electrospinning are of industrial and scientific interest due to their long lengths, small diameters, and high surface area per unit volume. The process is complex with the resulting jet (fiber) diameter being influenced by numerous material, design, and operating parameters. Nanofiber properties can vary dramatically given the many variables that may influence the process such as the polymer (type, molecular weight), solvent (types, vapor pressure, diffusivity in air), additives (surfactants, salts), polymer concentration, solution properties (rheological behavior, relaxation time, viscosity, surface tension, electric conductivity and

dielectric permittivity), electric field (strength, geometry), solution feed rate, nozzle orifice diameter, distance from nozzle to collector, and ambient conditions (relative humidity, temperature, etc.)[18].

In this study, firstly Poly(acrylonitrile-co-vinyl acetate)/polypyrrole composite particles with uniform size and morphology have been synthesized using one step polymerization that involves swelling and coating of polypyrrole (PPy) into P(AN-co-VAc) latex particles. As an initial, free radical copolymerization of acrylonitrile (AN) - vinyl acetate (VAc) was synthesized by emulsion polymerization method using ammonium persulfate (APS) and Sodium dodecylbenzenesulfonic acid (DBSA). P(AN-co-VAc)/PPy composites were obtained by adding the pyrrole monomers into the continued reaction. Composites were characterized in terms of chemical composition, surface morphology, particle size, conductivity, thermal and mechanical properties by using NMR, Fourier Transform Infrared - Attenuated Total Reflectance spectrophotometer (FTIR-ATR), Scanning Electron Microscope (SEM), Parstat Electrochemical Analyser via EIS measurement,UV-Visible Spectrophotometer, Differential Scanning Calorimeter (DSC) and Dynamic Mechanical Analyser, DMA.

The second part of this study, the electrospinning method was applied to produce Nanofibers of P(AN-co-VAc) copolymer and P(AN-co-VAc)/PPy composites. Moreover, relationship between Py content, viscosity and fiber diameter were examined and increasing of Py content lead to decreasing nanofiber diameter is determined. Morphological properties of nanofibers were investigated by scanning electron microscopy (SEM) and atomic force spectroscopy (AFM).

2. THEORETICAL PART

2.1 Acrylonitrile, Polyacrylonitrile and Poly(acrylonitrile-co-vinyl acetate)

The first synthesis of AN was made in 1893 by Moureu [19].

By the dehydration of ethylene cyanhydrine (1-cyanoethanol) or acrylamide, AN was first synthesized. Ethylene cyanhydrine was used as starting material for the industrial processes of AN production, but since 1960 practically the entire AN production has been based on catalytic ammonoxidation of propene [20].

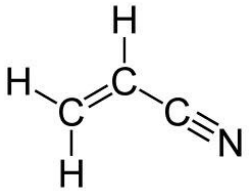

Figure 2.1: General formula of acrylonitrile.

Respect to the other vinyl polymerization reactions, AN have different characteristic properties. AN is soluble in most organic solvents and in water. The nevertheless, solubility of PAN differs from its monomer. It is insoluble in most common organic solvents, in water, and also in its monomer. Therefore, the polymerization reaction often becomes heterogeneous even at low conversions and monomer concentrations, and the borders between emulsion and suspension polymerization are not well defined. Heterogeneous AN polymerization shows autoacceleration when an insufficient amount of a surfactant is used. Furthermore, there is obviously no consensus among the authors reporting on AN polymerization as far as use of the terms solution polymerization, dispersion polymerization, and precipitation polymerization is concerned, especially in aqueous systems [21].

Polyacrylonitrile (PAN) is a commercially important polymer because of its unique and well-known properties including hardness and rigidity, chemical resistance, compatibility with certain polar substances, and low gas permeability [22]. PAN is usually prepared by radical polymerization without control over molecular dimension

and structure [23]. PAN is highly polar with strong interchain interactions through nitrile groups and it decomposes before melting [24-25]. During the heat treatments of homo and copolymers of acrylonitrile, instead of melting, some exothermic reactions, such as cyclization of nitrile groups takes place which lead to formation of ladder like structure. PAN has a large magnitude of the dipole moments of the CN lead to strong intrachain and interchain interactions through secondary bonding. Therefore, incorporating a number of flexible comonomers weakens the dipolar interactions among CN and thereby decreases melting point or increases decomposition temperatures of the PAN based copolymers [26].Hence, it is important to consider the effect of comonomer on the thermal behaviour of PAN based copolymers [27].

Table 2.1: Typical free radical chain copolymerization reactivity ratios at 60°C [28].

M_1	M_2	r_1	r_2	r_1r_2
Acrylonitrile	Butadiene	0.25	0.33	0.08
	Ethyl acrylate(50^oC)	1.17	0.67	0.78
	Maleic anhydride	6	0	0
	Methyl methacrylate	0.13	1.16	0.15
	Styrene	0.04	0.41	0.16
	Vinyl acetate	4.05	0.06	0.24
	Vinyl chloride	3.28	0.02	0.07

The reactivity ratios may be determined by an analysis of the change in composition of the feed during the very early stages of polymerization. Typical free radical chain copolymerization reactivity ratios of acrylonitrile copolymers are listed in Table 2.1. AN is copolymerized with one or two comonomers, such as acrylates, methacrylates, styrene, and particularly vinyl acetate (VAc). The copolymer of AN and VAc can be used either as a plastic (VAc>15 wt%) or as microfibers (VAc<15 wt%) [29]. AN provides the copolymer with good processability, electrochemical and thermal stability; VAc provides the excellent mechanical stability [30]. AN–VAc copolymers have the significant importance in the commercially available acrylic fibers due to

their thermal behavior and are also of interest as precursors in the production of high strength carbon fibers [31-32].

2.2 Emulsion Polymerization

Emulsion copolymers are of technological importance as they are extensively used in leather, paper, textile, paint, carpet, and adhesives, and for biomedical applications. The compositions of the copolymers are of paramount importance, as they dictate the end-use applications. [33].

Emulsion polymerization is a heterogeneous, free-radical polymerization process which has wide industrial application in the production of polymer colloids or latices of several different types of polymers: poly(vinyl acetate), vinyl acetate copolymers, acrylate ester copolymers, polybutadiene and butadiene-styrene copolymers, poly(vinyl chloride) and vinyl chloride copolymers, vinyledene chloride copolymers, polyethylene, acrylamide copolymers [34-38].

In emulsion polymerization, monomer is added into the aqueous mixture including a water soluble initiator and a surfactant (detergent or soap). Surfactant has long hydrocarbon chains with a polar functional groups at one end. In water, the surfactants molecules organize themselves in to micelles. The hydrocarbon chains, being hydrophobic (water-hating) mix together inside the micelles. The water soluble, polar functional groups (hydrophilic or water-loving) on the ends of the chains form the outer surface of micelles. The polar end groups keep the micelles suspended in water. The monomer, which is not very soluble in water, diffuses from large monomer droplets through the water to the micelles. Initiating radicals are generated and migrate to the surface of the micelles, where they encounter monomers. Polymerization occurs inside the monomer-swollen micelles by essentially a bulk polymerization process. The micelles containg polymer molecules, called as polymer particles, continue to grow as fresh monomer diffuses in constantly. The rates of emulsion polymerization are very high, and reactions are typically run at very high monomer concentrations. The result is a white emulsion resembling milk, called as latex. Latexes have low viscosities and often used directly without purification or isolation. The process is summarized in figure 2.2.

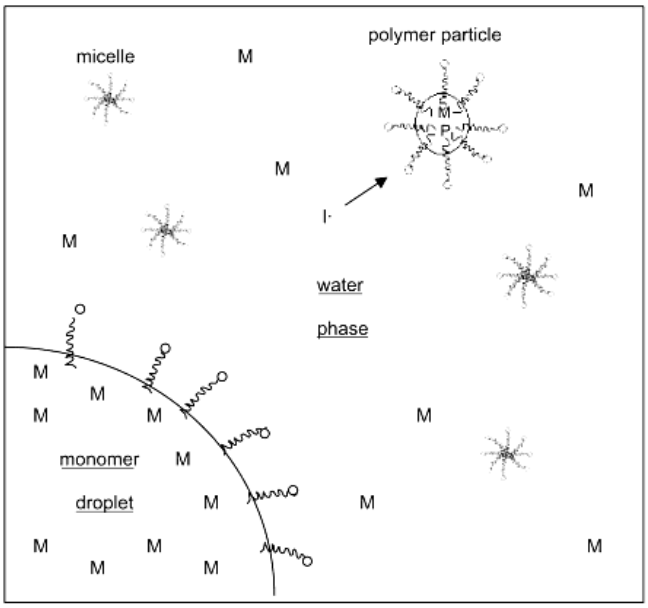

Figure 2.2: Schematic view of emulsion polymerization [39].

Basic species present in an emulsion polymerization is shown in figure 2.2 where I, M, P, and represent the radical initiator, monomer, polymer and, surfactant molecule: circle represents polar functional group; squiggly line represents long alkyl chain respectively [39].

After the ~15% conversion of monomer to polymer, all the micelles become polymer particles are obtained in the micelles. Later the 40-60% monomer conversion is observed, droplet phase of monomer remarkablely began to disappear. Termination occurs when a radical (usually from the initiator) diffuses in from the aqueous phase.

Once an initiator radical enters a polymer monomer particle and initiates a chain, the latter must continue to propagate with the available monomer until another radical enters the same particle. In this way, the rate of chain termination is actually controlled by the rate of entry of radicals into the particles, and this generally inreases the lifetime of the growing chains, and hence the chain length. The termination step in an emulsion polymerization is controlled by the rate of arrival of radicals at the polymer particles, which depends only an the concentration of surfactant [40,41]. Compared with other systems, the possibility of preparing an emulsion with a high PAN content is rather limited. This is caused by the comparatively high water solubility of AN, the poor solubility of PAN in its monomer (which is required for the formation of latex particles), the high polarity of PAN, and the strong attractive forces between the nitrile groups on the surface of the

polymer particles. Therefore, strong emulsifiers are required in high concentrations [42-45].

Another possibility for producing stable PAN emulsions is to incorporate ionic or hydrophilic groups such as sulfonate or carboxylate groups into the polymer. This can be done by copolymerizing AN with monomers with adequate functions [46,47].

These disadvantages of the emulsion polymerization of AN are soon overcome when the comonomer content rises. Thus for the production of modacrylics (15 to 50% comonomer), emulsion polymerization is as advantageous as it is for common vinyl polymerization [48-52].

2.3 Free Radical Polymerization

Free radical polymerization is a rapid reaction which consists of the characteristic steps of initiation, propagation, and termination. Free radical initiation can occur through application of heat (thermal), UV and visible light (photochemical), ionizing light, redox reagents, electricity (electrochemical), etc., that is any process that creates the essential free radicals. Steps of radical vinyl polymerization is given below.

2.3.1 Chain Initiation

The chain initiation step involves two reactions. In the first step, a radical is produced by any one of a number of reactions. The most common is the homolytic decomposition of an initiator species I to yield a pair of initiator or primary radicals R*:

$$I \xrightarrow{k_d} 2R^* \qquad \textbf{(2.1)}$$

where k_d is the rate constant for the catalyst dissociation. The second step involves the addition of this radical R* to the first monomer molecule to produce the chain-initiating species P_1*:

$$R^* + M \xrightarrow{k_i} P_1^* \qquad \textbf{(2.2)}$$

where k_i is the rate constant for the second initiation step.

2.3.2 Chain Propagation

Propagation consists of the growth of P_1* by the successive addition of large number of monomer molecules (M) The addition steps may be represented as follows:

$$P_1^* + M \xrightarrow{k_p} P_2^* \quad \textbf{(2.3)}$$

$$P_2^* + M \xrightarrow{k_p} P_3^* \quad \textbf{(2.4)}$$

$$P_n^* + M \xrightarrow{k_p} P_{n+1}^* \quad \textbf{(2.5)}$$

where kp is the propagation rate constant.

Propagation is a bimolecular reaction which takes place by the addition of the free radical to another molecule of monomer, and by many repetitions of this step as represented in Eqs. (2.3)-(2.5). The propagation rate constant is generally considered to be independent of the chain length.

2.3.3 Chain Termination

Chain propagation to a high-molecular-weight polymer takes place very rapidly.

At some point, the propagating polymer chain stops growing and terminates. The two different types of termination can be occurred. One of them is combination (coupling); two propagating radicals react with each other by combination (coupling) to form a dead polymer. Other one is disproportionation; this step involves a hydrogen radical that is beta to one radical center transferred to another radical center to form two dead polymer chains (one saturated and one unsaturated).

Termination can also occur by a combination of coupling and disproportionation.

The two different types of termination may be represented as follows:

$$P_m^* + P_n^* \xrightarrow{k_{tc}} P_{m+n}^* \quad \textbf{(2.6)}$$

$$P_m^* + P_n^* \xrightarrow{k_{t,d}} P_m + P_n \quad \textbf{(2.7)}$$

Chain transfer is a chain-stopping reaction. It results in a decrease in the size of the propagating polymer chain. This effect is due to the premature termination of a growing polymer chain by the transfer of a hydrogen or other atom from some

compound present in the system (i.e., monomer, solvent, initiator, etc.). These radical displacement reactions are termed chain transfer reactions and may be presented as

$$P_n^* + M \xrightarrow{k_{tr,m}} P_n + P_1^* \quad \textbf{(2.8)}$$

$$P_n^* + P_m \xrightarrow{k_{tr,p}} P_n + P_m^* \quad \textbf{(2.9)}$$

where $k_{tr,m}$ and $k_{tr,p}$ are the chain transfer rate constant. The reinitiation or participation in termination reactions may be occurred by the P_1^* and P_m^* respectively, in the free radical chain polymerization to form linear and branched polymer chains [53,54].

2.4 Conductive Polymers

Following the successful synthesis of conducting polyacetylene in 1977 by Shirakawa *et al.*, electrically conducting polymers have generated tremendous interest due to their potential applications in batteries, electrochromic display devices, sensors etc. Electrically conducting organic polymers are a novel class of 'synthetic metals' that combine the chemical and mechanical properties of polymers with the electronic properties of metals and semiconductors [55,56].

It was first noted in 1968 that pyrrole could be polymerized electrochemically, and in 1973 that it could be readily polymerized chemically by a wide variety of oxidizing agents to give a black conducting powder. Since this time, research activity in the field has continued to proceed at a constantly increasing pace, although the greatercost of pyrrole as compared to aniline, has tended to make it less attractive for many potential technological applications [57,58].

The great advances in the field of polyaniline and polypyrrole since the mid-1980's have resulted from the ability to reproducibly synthesize the pure polymers in a known oxidation state, with a known molecular weight (where applicable) with a known degree of doping. Pure materials have permitted meaningful physical studies involving structure, conductivity, magnetic and optical phenomena which have resulted in a better understanding of factors controlling conductivity and transport phenomena in general [59].

2.4.1 Synthesis of Polypyrrole

Polypyrroles (PPy's) are formed by the oxidation of pyrrole or substituted pyrrole monomers. In the vast majority of cases, these oxidations have been carried out by either [60] electropolymerization at a conductive substrate (electrode) through the application of an external potential or [61] chemical polymerization in solution by the use of a chemical oxidant. Photochemically initiated and enzyme-catalyzed polymerization routes have also been described but are less developed. These various approaches produce polypyrrole (PPy) materials with different forms of chemical oxidations generally produce powders, whereas electrochemical synthesis leads to films deposited on the working electrode, and enzymatic polymerization gives aqueous dispersions. The conducting polymer products also possess different chemical/electrical properties [63]. In this study, the chemical polymerization of pyrrole was discussed.

Chemical Polymerization

The range of dopant counterions (A−) that may be incorporated into the PPy backbone during polymerization has also, until recently, been generally limited to ions associated with the oxidant. However, chemical polymerization remains of interest for processing purposes because it may be easier to scale up this batch process and it results in the formation of powders or colloidal dispersions. The most widely used chemical oxidants have been ammonium persulfate, $(NH_4)_2S_2O_8$, and $FeCl_3$, although hydrogen peroxide and a range of transition metal salts have also been employed. The use of H_2O_2 (with Fe^{3+} catalyst) is attractive environmentally, as the only by-product is water.

The vast majority of chemical polymerizations of pyrrole have been carried out between 0°C and room temperature. The dopant anions incorporated into conducting PPy's are positioned interstitially between the polymer chains and, as discussed earlier for electropolymerization, their nature consequentially influences both the polymerization process and the properties of the resultant polymers. In initial chemical polymerization studies, the incorporated anions were limited to those arising from the oxidant employed; for example, $FeCl_3$ and $(NH_4)_2S_2O_8$ oxidants provided Cl^- and HSO_4^-/SO_4^{2-} counterions, respectively.

Both chemically and electrochemically synthesized PPy's are typically insoluble in water and organic solvents, and are infusible because of strong intermolecular and intramolecular interactions of their polymer chains. There has been intense research over the past decade to overcome this serious hindrance to their processibility and subsequent utilization. More recently, it has been found that anions such as polyelectrolytes and surfactant- like anions, for example, dodecylbenzenesulfonate (DBSA), can be inserted directly into PPy products during polymerization in competition with anions arising from the oxidant [64].

Counterion-Induced Solubilization

An important breakthrough in PPy chemistry was the discovery by Lee and coworkers [62] in 1995 of a chemical polymerization route to an unsubstituted PPy that was soluble in organic solvents. They exploited the surfactant-like qualities of added dodecylbenzenesulfonate (DBSA; figure 2.3) as a dopant anion to solubilize PPy formed during oxidation of pyrrole by aqueous $(NH_4)_2S_2O_8$. The PPy/DBSA product, isolated as a black powder in 42% yield after 40 h reaction at 0°C, was very soluble in *m*-cresol, and could be dissolved in weakly polar solvents such as chloroform and dichloromethane by the addition of an equimolar amount of dodecylbenzenesulfonic acid. A film cast from chloroform solution exhibited an electrical conductivity of 5 S cm−1, and its UV-visible spectrum was similar to that of electrochemically deposited PPy. The solubilizing ability of the DBSA dopant is believed to arise from the longchain dodecyl group reducing the interactions between the PPy chains as well as assisting solvation by the organic solvents [65].

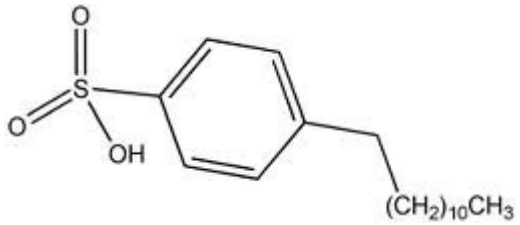

Figure 2.3: DBSA.

Colloidal PPy Dispersions

Colloidal PPy's prepared in aqueous solution are generally spherical. Particle size is very dependent on the synthetic conditions (stabilizer, oxidant, etc.), with sizes between 30 and 445 nm being described by Armes and Vincent. The electrical

conductivities of the PPy colloids are frequently a few orders of magnitude lower than those observed for macroscopically precipitated PPy's [66].

2.4.2 Properties of Polypyrrole

Polypyrrole (PPy) is one of the most important conductive polymers because of its high stability, electronic conductivity, ion exchange capacity and biocompatibility [67-71].

But it is hard and brittle with poor flexibility [72-74]. Some methods have been developed to increase mechanical properties such as making composites with appropriate polymers.

The heteroaromatic and extended *p*-conjugated backbone structure of PPy provide it with chemical stability and electrical conductivity, respectively. However, the π-conjugated backbone structure is not sufficient to produce appreciable conductivity on its own. Partial charge extraction from PPy chain is also required, which is achieved by a chemical or an electrochemical process referred to as doping. The conductivity of the neutral PPy are remarkably changed from an insulating regime to a metallic one by doping [75,76].

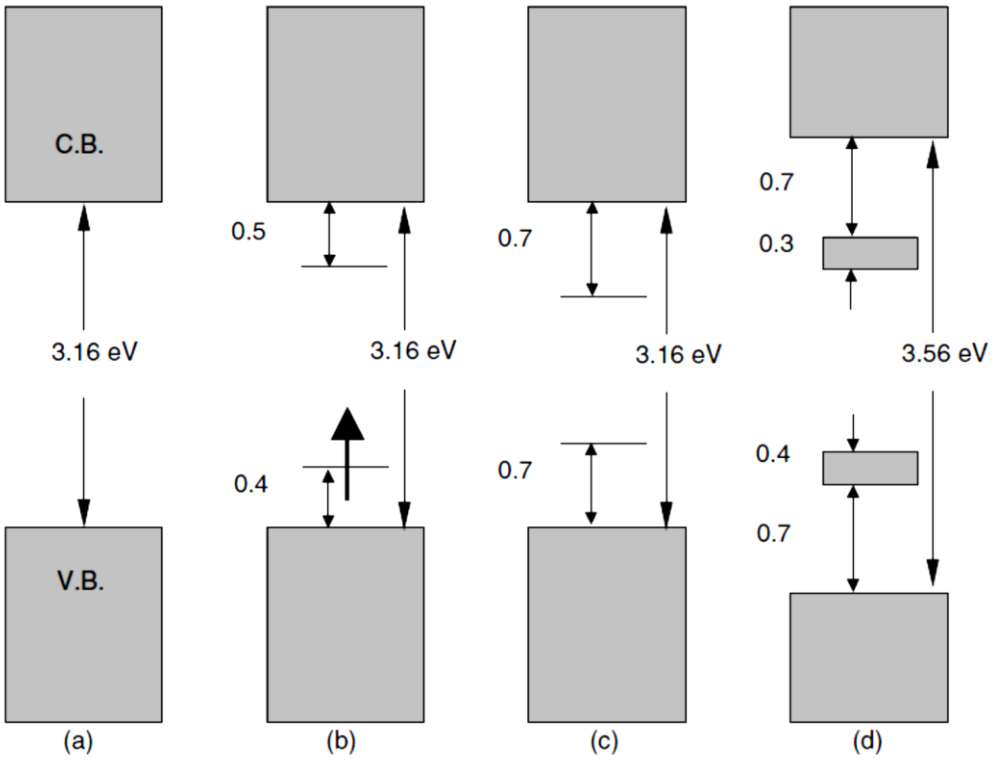

Figure 2.4: Electronic energy diagrams for (a) neutral PPy, (b) polaron, (c) bipolaron, and (d) fully doped PPy.

The band gap of neutral PPy is reported to be 3.16 eV, which is too wide for electrons to transfer from the valence to the conduction band at room temperature. The PPy chain is, however, simultaneously doped during polymerization [77]. Neutral PPy, polaron, bipolaron and fully doped PPy electronic energy diagrams are shown in Figure 2.4.

Upon extraction of a negative charge from a neutral segment of a PPy chain by the doping process, a local deformation to the quinoid structure occurs (Figure 2.5b), since it is favored energetically. In combination with the quinoid structure, the positive charge and the unpaired spin are referred to as a polaron (Figure 2.5b). Referring to Figure 2.4b, the formation of a polaron induces two new intermediate states (bonding and antibonding) within the band gap while the unpaired electron occupies the bonding (low energy) state, thus giving the polaron a spin of 1=2.

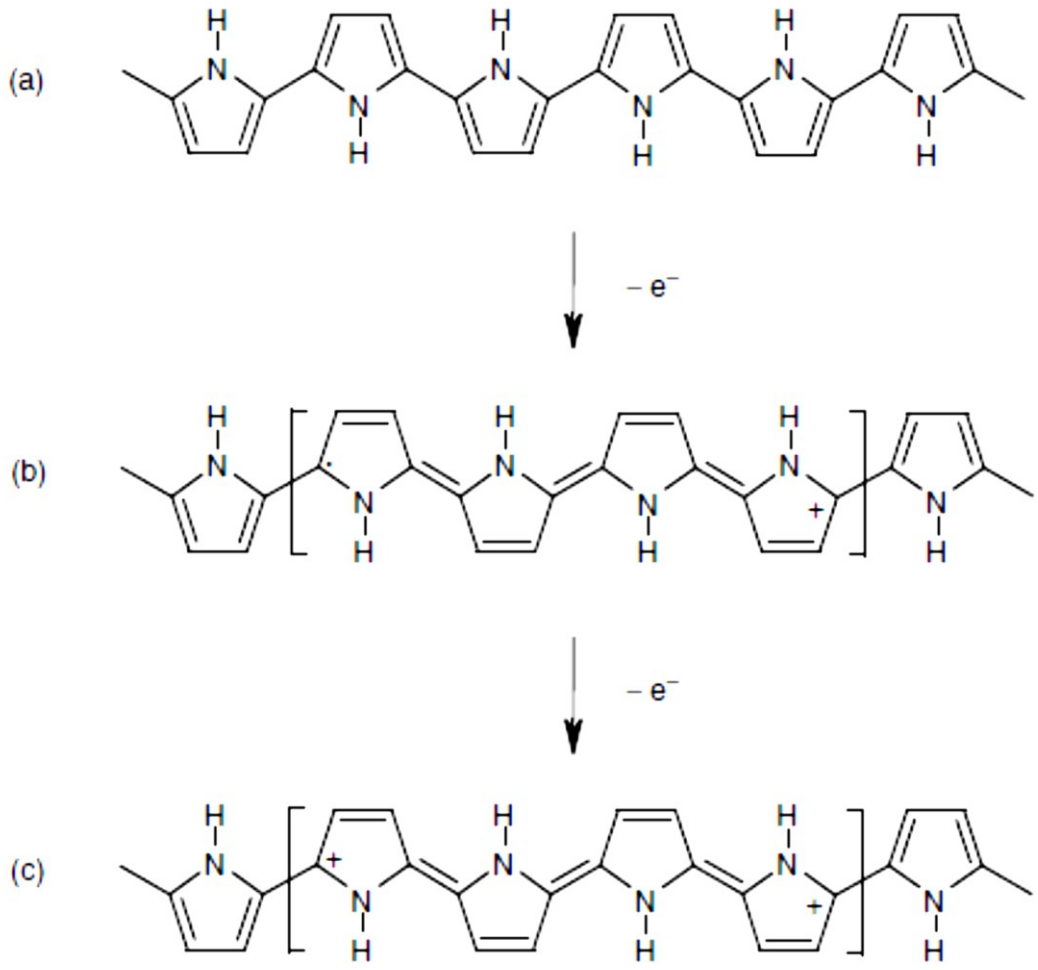

Figure 2.5: Electronic structures of (a) neutral PPy, (b) polaron in partially doped PPy and (c) bipolaron in fully doped PPy [78].

As oxidation continues further, another electron has to be removed from a PPy chain that already contains a polaron, resulting in the formation of a bipolaron which is energetically preferred to the formation of two polarons. A bipolaron is known to extend over about four pyrrole rings (Figure 2.5c). The bipolaron states lie further from the band edges (Figure 2.4c). The lower energy state of the bipolaron is empty; thus the species has a zero spin. As the degree of oxidation increases, the bipolaronic

energy state overlaps, resulting in the formation of narrow intermediate band structures (Figure 2.4d). The energy diagram shown in Figure 2.4d corresponds to a doped state of about 33 mol%, which is close to the maximum value found in electrochemically oxidized PPy. The typical doping level of PPy is in the range of 20 to 40 mol% [78].

The UV-visible spectra of PPy's and their changes with varying doping levels have, in a number of cases, been correlated with the previous predictions, as first discussedby Bredas and coworkers [79]. In general, highly doped PPy's exhibit two characteristic bipolaron bands at 1.0 and 2.6 eV (1240 and 475 nm) as well as a π–π^* band [80,81]. Marked changes in their UV-visible-NIR spectra occur for the recently discovered [82] "soluble" PPy's when the organic solvent is varied [83-86]. For example, the bipolaron band observed at 475 nm for PPy/DBSA (DBSA = dodecylbenzenesulfonate) in chloroform solvent undergoes a large blue shift to 425 nm with *m*-cresol or dimethyl sulfoxide (DMSO) as solvent [87,88].

2.4.3 Application areas of conductive polymers

Conducing polymers have very wide potential applications (Figure 2.6). Conducting polymers are currently used for metallization of plated through-holes for printed circuit board technology in a number of companies worldwide. Conducting-polymer-based coatings have been developed that offer excellent ESD protection and numerous advantages over materials in current use. A number of the coating formulations are either already commercial or in the process of being rendered commercial. Corrosion protection of metals such as silver and copper using conducting polymers has also been shown to be quite promising [89].

Conducting polymers can in principle be considered as candidates for interconnection technology. The use of conducting polymers for wiring has been widely speculated upon since the emergence of these materials in the late 1970s.

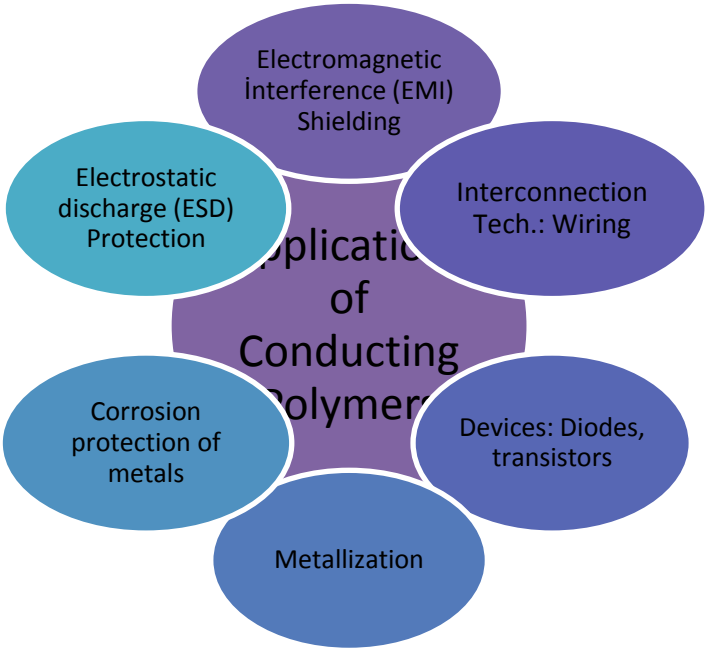

Figure 2.6: Overview of some application areas of conducting polymers.

For such an application, copper-like conductivity is necessary. Unfortunately, polyacetylene is the only conducting polymer that currently exhibits such conductivity, and its environmental instability and lack of processability preclude its use. A dramatic enhancement of the conductivity of some of the more processable and environmentally stable polymers is required before they can be realistically considered as viable conductors for interconnection technology [90-95].

2.5 Nanofiber

Recently, nano-scaled materials have been investigated with amazing increased interest due to their many advantages, such as large surface area and many active surface sites. Among different nano-scaled materials, nanofibers have been widely applied in industry due to the ease in production processes compared to other nano-materials.

Nanofibers, because of their unique properties, such as a small diameter, a high specific surface area (Figure 2.7), and the potential to incorporate active chemistry, have many applications [96-97].

Nanofibers are usually fabricated by the electrospinning method as a non-woven mat. Nonwoven fabrics are textile materials consisting of randomly oriented fibers

connected together by physical entanglements or bonds between individual fibers, without any knitting or stitching. These non-woven nanofibers are the primary alternative for traditional textiles as filtration media, energy storage media, hygienic and health/personal care textiles, thermal and sound insulating materials, ecological materials, building materials, geo-textiles and automotive textiles [98].

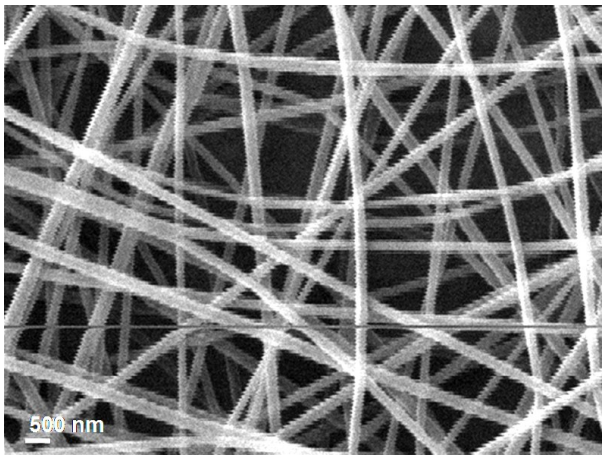

Figure 2.7: SEM image of nanofibers from previous studies[160].

2.6 Electrospinning

Electrospinning (also called electrostatic fiber spinning) has been one of the promising processes to produce continuous nano-scale fibers from both synthetic and natural polymers. Electric forces are used to form fibers from material solutions or melts in the electrospinning process. Studies on electrically driven liquid jets were initially started in 19th century, and electrospinning of polymer fibers was first patented by Formhals in 1934 [99].

Electrospinning has rapidly changed fiber making from a capital intensive, large scale process to a low cost, broadly applicable method that manufactures fibers on a laboratory bench, to serve diverse needs ranging from materials science and technology to life sciences and clinical medicine. The high ratio of surface area to mass is a primary characteristic of nanofibers. Electrospinning depends on the complex interplay of surfaces, shapes, rheology, and electrical charge. These phenomena interact in different ways to create electrified jets of polymer solutions and molten polymers. The charges are usually carried by ions, which may move through the fluid faster, commensurate with, or slower than the shape of the fluid changes. For a fixed quantity of fluid, the Coulomb repulsion between the charged

ions favors the creation of shapes such as a jet, while the surface tension of the fluid favors sphere-like shapes with smaller surface area per unit mass. When the electrical potential of the surface is increased to a sufficiently high value, the electrical forces act in opposition to, and dominate the surface tension of the fluid. A charged jet of fluid is then ejected.

The electrical charge that is important in electrospinning is excess or uncompensated charge, usually in the form of positive or negative ions. Although all ionic solutions contain charged molecules or ions, the solution is electrically neutral because the number of positive and negative ions is exactly equal. The essential excess ions are usually created near the interface between a metallic conductor and the molecules in the solution. Electrons moving into the solution from the metal create excess negative ions in the solution. Electrons moving from the solution into the metal leave excess positive ions in the solution. Once created, the ions move by diffusive and convective processes [100] to reduce the repulsive interactions between the similarly charged excess ions and to maintain the same electrical potential everywhere on the surface of the fluid body.

The convenience of making fibers by electrospinning many kinds of polymers, on a laboratory bench, with inexpensive machinery makes nanofibers of many polymers available for a wide variety of possible applications. Dramatic improvements in filtration technology, based on the use of nanofibers, have occurred. Many molecules, particles, and biological structures can be sequestered and protected inside nanofibers, while remaining accessible for use when needed. Nanofibers can be used as convenient packages and supports for reagents and catalysts. Novel fabrics and structures can be made [101].

2.6.1 Electrospinning process

Electrospinning, a spinning technique, is a unique approach using electrostatic forces to produce fine fibers from polymer solutions or melts and the fibers thus produced have a thinner diameter (from nanometer to micrometer) and a larger surface area than those obtained from conventional spinning processes. Furthermore, a DC voltage in the range of several tens of kVs is necessary to generate the electrospinning. Various techniques such as electrostatic precipitators and pesticide sprayers work similarly to the electrospinning process and this process, mainly based

on the principle that strong mutual electrical repulsive forces overcome weaker forces of surface tension in the charged polymer liquid [102]. Currently, there are two standard electrospinning setups, vertical and horizontal. The Experimental setup of electrospinning shown in Figure 2.8.

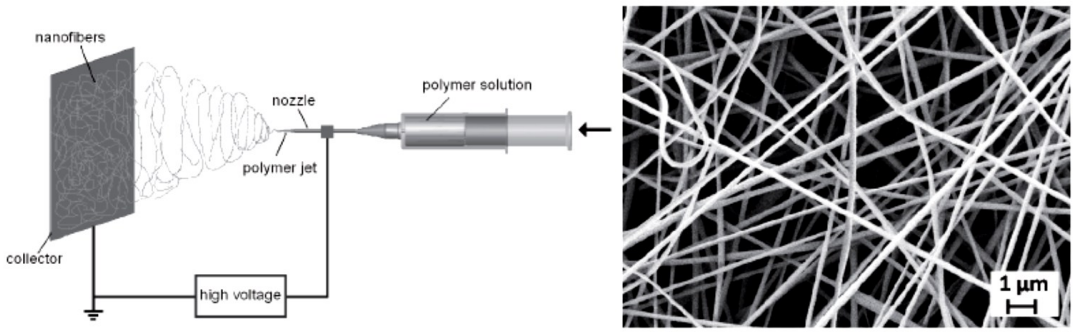

Figure 2.8: Typical setup of electrospinning device [103].

Basically, an electrospinning system consists of three major components: a high voltage power supply, a spinneret (e.g., a pipette tip) and a grounded collecting plate (usually a metal screen, plate, or rotating mandrel) and utilizes a high voltage source to inject charge of a certain polarity into a polymer solution or melt, which is then accelerated towards a collector of opposite polarity [104,105]. Most of the polymers are dissolved in some solvents before electrospinning, and when it completely dissolves, forms polymer solution. The polymer fluid is then introduced into the capillary tube for electrospinning. However, some polymers may emit unpleasant or even harmful smells, so the processes should be conducted within chambers having a ventilation system [106].

In the electrospinning process, a polymer solution held by its surface tension at the end of a capillary tube is subjected to an electric field and an electric charge is induced on the liquid surface due to this electric field. When the electric field applied reaches a critical value, the repulsive electrical forces overcome the surface tension forces. Eventually, a charged jet of the solution is ejected from the tip of the Taylor cone and an unstable and a rapid whipping of the jet occurs in the space between the capillary tip and collector which leads to evaporation of the solvent, leaving a polymer behind [107-109].

The jet is only stable at the tip of the spinneret and after that instability starts. Thus, the electrospinning process offers a simplified technique for fiber formation [110].

2.6.2 Effects of parameters on electrospinning

The electrospinning process is solely governed by many parameters, classified broadly into solution parameters, process parameters, and ambient parameters.

Each of these parameters significantly affect the fibers morphology obtained as a result of electrospinning, and by proper manipulation of these parameters we can get nanofibers of desired morphology and diameters [111].

2.6.3 Solution parameters

2.6.3.1 Viscosity

Solution viscosity plays an important role in determining the fiber size and morphology during spinning of polymeric fibers. It has been found that with very low viscosity there is no continuous fiber formation and with very high viscosity there is difficulty in the ejection of jets from polymer solution, thus there is a requirement of optimal viscosity for electrospinning [112]. At very high viscosity polymer solutions usually exhibit longer stress relaxation times, which could prevent the fracturing of the ejected jets during electrospinning. An increase in solution viscosity or concentration gives rise to a larger and more uniform fiber diameter [113]. For solution of low viscosities, surface tension is the dominant factor and just beads or beaded fibers are formed while above a critical concentration, a continuous fibrous structure is obtained and its morphology is affected by the concentration of the solution [114].

2.6.3.2 Surface tension

Surface tension, more likely to be a function of solvent compositions of the solution plays a critical role in the electrospinning process and by reducing the surface tension of a nanofiber solution; fibers can be obtained without beads. Different solvents may contribute different surface tensions. Generally, the high surface tension of a solution inhibits the electrospinning process because of instability of the jets and the generation of sprayed droplets [115]. Basically, surface tension determines the upper and lower boundaries of the electrospinning window if all other variables are held constant [116-118].

2.6.3.3 Concentration

There should be an optimum solution concentration for the electrospinning process, as at low concentrations beads are formed instead of fibers and at high concentrations the formation of continuous fibers are prohibited because of the inability to maintain the flow of the solution at the tip of the needle resulting in the formation of larger fibers [119]. Researchers have attempted to find a relationship between solution concentration and fiber diameter and they found a power law relationship, that increasing the concentration of solution, increases the fiber diameter with gelatin electrospinning [120-121].

2.6.3.4 Molecular weight

Molecular weight of the polymer has a significant effect on rheological and electrical properties such as viscosity, surface tension, conductivity and dielectric strength [122]. This is the other important solution parameter that affects the morphology of electrospun fiber and generally high molecular weight polymer solutions have been used in electrospinning as they provide the desired viscosity for the fiber generation. It has been observed that too low a molecular weight solution tends to form beads rather than fibers and a high molecular weight solution gives fibers with larger average diameters. Molecular weight of the polymer reflects the number of entanglements of polymer chains in a solution, thus solution viscosity. Chain entanglement plays an important role in the processing of electrospinning. It has been observed that high molecular weights are not always essential for the electrospinning process if sufficient intermolecular interactions can provide a substitute for the interchain connectivity obtained through chain entanglements, and using this principle, researchers have prepared oligomer-sized phospholipids from lecithin solutions into nonwoven membranes through electrospinning [123-124].

2.6.3.5 Conductivity/surface charge density

Polymers are mostly nonconductive, with a few exceptions of dielectric materials, and the charged ions in the polymer solution are highly influential in jet formation. Solution conductivity is mainly determined by the polymer type, solvent used, and the availability of ionisable salts. It has been found that with the increase of electrical conductivity of the solution, there is a significant decrease in the diameter of the electrospun nanofibers whereas with low conductivity of the solution, there results

insufficient elongation of a jet by electrical force to produce uniform fiber, and beads may also be observed. Researchers have showed that highly conductive solutions are extremely unstable in the presence of strong electric fields, which results in a dramatic bending instability as well as a broad diameter distribution [125].Generally, electrospun nanofibers with the smallest fiber diameter can be obtained with the highest electrical conductivity and it has been found that the there is drop in the size of the fibers is due to the increased electrical conductivity. It was observed that the jet radius varied inversely with the cube root of the electrical conductivity of the solution [126-134].

2.6.4 Processing parameters

Another important parameter that affects the electrospinning process is the various external factors exerting on the electrospinning jet. This includes the voltage supplied, the flow-rate, type of collector, and distance between the needle tip [135].

2.6.4.1 Applied voltage

The high voltage will induce the necessary charges on the solution and together with the external electric field, will initiate the electrospinning process when the electrostatic force in the solution overcomes the surface tension of the solution. Generally, both high negative or positive voltage of more than 6kV is able to cause the solution drop at the tip of the needle to distort into the shape of a Taylor Cone during jet initiation [136]. Depending on the feedrate of the solution, a higher voltage may be required so that the Taylor Cone is stable. The columbic repulsive force in the jet will then stretch the viscoelastic solution. If the applied voltage is higher, the greater amount of charges will cause the jet to accelerate faster and more volume of solution will be drawn from the tip of the needle. This may result in a smaller and less stable Taylor Cone [137]. When the drawing of the solution to the collection plate is faster than the supply from the source, the Taylor Cone may recede into the needle [138].

Applied voltage has also effects on the morphology and the resultant fibers. Increase in the applied voltage results with a decrease in the fiber diameter. Generally, high voltage results with higher bead formation, but increased jet stretching leads to fewer amounts of beads [139]. At lower voltage, due to the weaker electrostatic force, flight time may last longer. Longer flight time lets the jet to elongate and stretch

stronger and longer resulting with reduced fiber diameter. Wang and his research team measured both jet diameter and fiber diameter and investigated the effect of voltage difference [140]. They found out that both jet diameter and fiber diameter decreased slightly. Also, better chain orientation within electrospun fibers was seen by an increase in the applied voltage. A proportionality relation between applied voltage and fiber diameter was reached in a study [141].

2.6.4.2 Flow rate

The flow rate of the polymer from the syringe is an important process parameter as it influences the jet velocity and the material transfer rate. A lower feed rate is more desirable as the solvent will get enough time for evaporation [142]. There should always be a minimum flow rate of the spinning solution. It has been observed that the fiber diameter and the pore diameter increases with an increase in the polymer flow rate in the case of polystyrene (PS) fibers and by changing the flow rate, the morphological structure can be slightly changed. Few studies have systematically investigated the relationship between solution feed or flow rate on fiber morphology and size [143-144].

If the flowrate is at the same rate which the solution is carried away by the electrospinning jet, there must be a corresponding increased in charges when the flowrate is increased. Thus there is a corresponding increase in the stretching of the solution which counters the increased diameter due to increased volume. Due to the greater volume of solution drawn from the needle tip, the jet will takes a longer time to dry. As a result, the solvents in the deposited fibers may not have enough time to evaporate given the same flight time. The residual solvents may cause the fibers to fuse together where they make contact forming webs. A lower flowrate is more desirable as the solvent will have more time for evaporation [145].

2.6.4.3 Distance

The distance (the distance from the terminus of the capillary tip to the surface of the collector) defines the strength of the electric field as well as the time available for evaporation of the solvent before the nanofibers reach the collector surface. Increasing the distance, leaving other parameters constant, generally reduces fiber diameters [146]. Reducing the distance does not affect size and shape of the fibers, but, inhomogeneously distributed beads can be observed [147]. These beads can be

due to increase in the electric field strength. If the distance between the tip and the collector is longer, solution jet finds more time for the evaporation of the solvent and jet can be stretched sufficiently before it lands to the collecting media. Increasing the working distance enhances both the number of beads and the density of the fibers [148]. Jet diameter dependence on the working distance is studied [149].

2.6.4.4 Effect of collector

In the electrospinning process, usually conductive material is used to cover collecting media. Aluminium foil is one of the most common conductive materials that are used for collection of fibers onto it.

One important aspect of the electrospinning process is the type of collector used. In this process, a collector serves as a conductive substrate where the nanofibers are collected. Generally, aluminium foil is used as a collector but due to difficulty in transferring of collected fibers and with the need for aligned fibers for various applications, other collectors such as, conductive paper, conductive cloth, wire mesh [150], pin [151], parallel or grided bar [152], rotating rod, rotating wheel [153], liquid non solvent such as methanol coagulation bath [154] and others are also common types of collectors nowadays. With less conductive area, there was generation of beaded fibers because of the less surface area. In another study they compared wire screen with aluminium foil and wire screen without aluminium foil in the same conductive area and found that pure wire screen is a better collector for fiber collection because with the use of wire screen the transfer of fibers to other substrates became easy. The fiber alignment is determined by the type of the target/collector and its rotation speed [155].

3. EXPERIMENTAL PART

3.1 Materials

Acrylonitrile (Dow, 99.5>%) vinyl acetate (Innovenne, 99.5>%) were provided by the Aksa Acrylic Factory of Turkey. Ammonium persulfate (APS) was Merck product. Sodium dodecyl benzene sulfonic acid salt was purchased from Sigma Aldrich. Dimethylformamide (DMF), methanol and ethanol were all Merck reagents. The Pyrrole (Py) was an Aldrich reagent. All these reagents were used as received.

3.2 Synthesis of P(AN-co-VAc) Copolymer

P(AN-co-VAc) latex was prepared by emulsion polymerization technique. The typical process for obtaining latex is as follows: 10 g of a mixture of monomers of AN and VAc (70:30 wt AN:VAc) were dropped into the three-neck flask, the mixture was stirred with distilled water during 20 minutes. Monomers were shown in Figure 3.1. Then, 0.5 g emulsifier sodium dodecyl benzene sulfonic acid (DBSA) was dissolved in 60 mL water. After that, DBSA was added to a stirred aqueous solution. 20 Minutes later, the dissolved 0.92 g APS in 20 mL distilled water was added to the flask. The copolymerization was carried out in a flask equipped with a stirrer (700 rpm) and a condenser and the temperature was adjusted to 70 ^{o}C and continued for 3 h under stirring. Copolymer structure was shown in Figure 3.2.

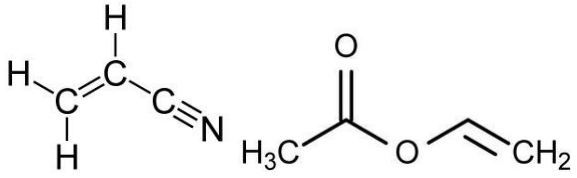

Acrylonitrile (AN) Vinyl Acetate (VAc)

Figure 3.1: Monomers used in synthesis of P(AN-co-VAc).

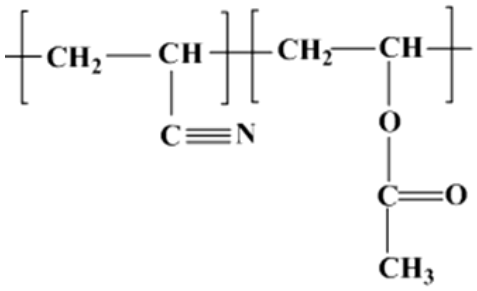

Figure 3.2: P(AN-co-VAc) structure.

Experimental setup of the polymerization was demonstrated in Figure 3.3. After the copolymerization, the prominent amount of polymer was washed and filtered with distilled water and ethanol, dried at room temperature. Residual emulsion was used for continued polymerization in order to obtain P(AN-co-VAc)/ PPy composites.

Figure 3.3: Experimental setup for synthesis of P(AN-co-VAc).

3.3 Coating of P(AN-co-VAc) Latex Particles with Polypyrrole

After obtaining P(AN-co-VAc) latex, the mixture was cooled for 30 min at room temperature and then, was transferred to 5 round-bottom flasks at equal volume. Four flasks were seperated for the coating processes. One of them is kept for comparison. Then, pyrrole monomer with different quantities were added dropwisely to the each seperated flasks at room temperature and the reaction continued for 18 hours. The content of the P(AN-co-VAc)/PPy composite was given in Table 3.1. Latex form of

composites were given in the Figure 3.4. After the 18 hours, reaction was stopped. Obtained composites in emulsion form were precipitated in methanol. Each product was filtered using filter paper, for the seperation of impurities and oligomers, the resultant products was washed with deionized water and ethanol, dried at room temperature. Composite structure was given in Figure 3.5.

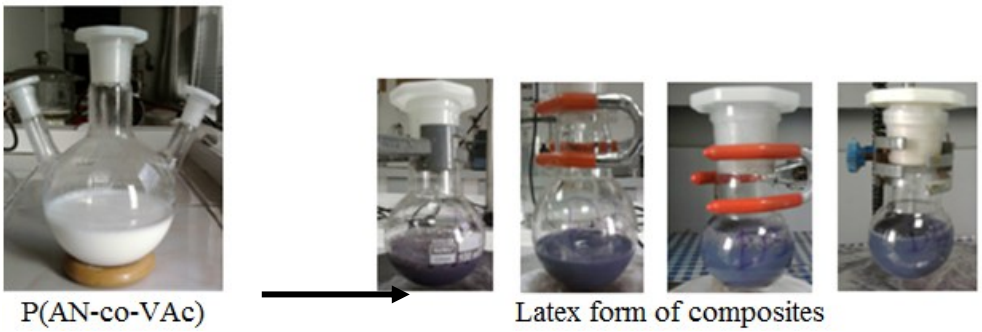

Figure 3.4: Latex form of P(AN-co-VAc), P(AN-co-VAc)@PPy1, P(AN-co-VAc)@PPy2, P(AN-co-VAc)@PPy3, P(AN-co-VAc)@PPy4, respectively.

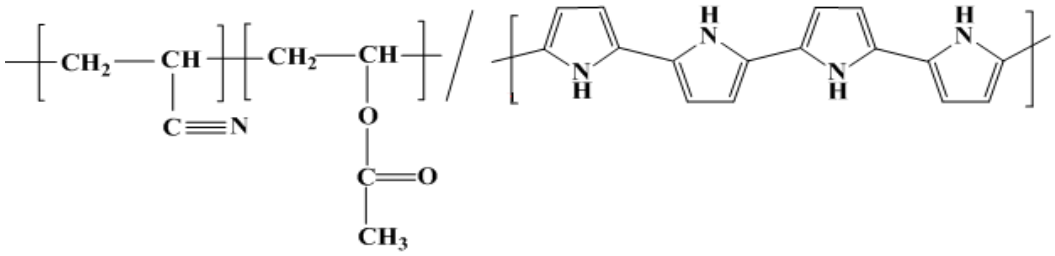

Figure 3.5: The structure of composite.

Table 3.1: Feed content of Py and content of PPy in composition.

Sample of Composite	Feed Py Monomer Mole Fraction (mol %)	PPy Mole Fraction (mol %)[a]
P(AN-co-VAc)@PPy$_1$	0.030	0.052
P(AN-co-VAc)@PPy$_2$	0.045	0.067
P(AN-co-VAc)@PPy$_3$	0.060	0.082
P(AN-co-VAc)@PPy$_4$	0.075	0.052

[a]:Determined from ^{1}H-NMR

3.4 Preparation of Electrospinning Solutions

Five series of P(AN-co-VAc)/PPy composite solutions with different content of pyrrole dissolved in DMF at room temperature. For each solutions were stirred at room temperature with the speed of 300 rpm at least 4 hour. View of electrospinning solutions were depicted in the Figure 3.6. The polymers were dissolved in DMF and were used to prepare nanofiber mats. The electrospinning conditions are shown in the Table 3.2. The electrospinning apparatus consists of a syringe pump (NE-500 model, New Era Pump Systems, Inc., USA) with feeding rate from 5.5 µL/h to 400 mL/h, high voltage DC power supplier generating positive DC voltage up to 50 kV DC power supply (ES50 model, Gamma High Voltage Inc., USA) and a grounded collector which is covered with aluminum foil. Solution was loaded into a syringe having 12 mm diameter and positive electrode was clipped onto the dispensing needle having 0.8 mm outer diameter. The feeding rate of the polymer solution was controlled by syringe pump.

Table 3.2: Electrospinning parameters for various composites.

Electrospinning Parameters	
Solution concentration	10 %
Applied voltage	15 kV
Tip-to-collector distance	15 cm
Feed rate	0.5 mL/h

Figure 3.6: View of electrospinning solutions of (a) P(AN-co-VAc) and (b) P(AN-co-VAc)@ PPy_4.

3.5 Electrospinning Process Setup

The metal collector was covered with an aluminum foil. The setup was kept in a plexiglass box for experimenter's safety. All experiments were carried out under atmospheric pressure and at room temperature. The positive electrode wire was hooked at the metal part of the needle and negative part of the electrode was attached to the metal collector 5 to 60 minutes of operation time was sufficient for the deposition of fibers on aluminum foil. A horizontal setup was chosen for electrospinning process. A picture that was captured during electrospinning is illustrated in Figure 3.7.

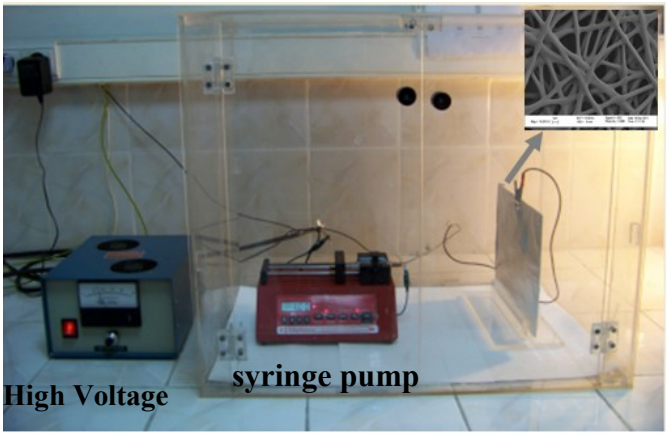

Figure 3.7: A representative view of electrospinning devices.

3.6 Characterization of P(AN-co-VAc) Copolymer and P(AN-co-VAc)/PPy Composites

The structure of the copolymers was characterized by means of ^{1}H NMR spectroscopy and Fourier Transform Infrared-Attenuated Total Reflectance (FTIR-ATR) spectroscopy, UV Visible Spectrophotometry.

- FTIR analysis of P(AN-co-VAc) and P(AN-co-VAc)@PPy_1, P(AN-co-VAc)@PPy_2, P(AN-co-VAc)@PPy_3, P(AN-co-VAc)@PPy_4 polymers in powder form and as nanofiber webs were carried out with FTIR-ATR reflectance spectrophotometer (Perkin Elmer, Spectrum One, with a Universal ATR attachment with a diamond and ZnSe crystal) (Figure 3.8).

Figure 3.8: Perkin Elmer FTIR-ATR spectrophotometer.

- ^{1}H NMR spectroscopy by using 250 MHz Bruker AC Aspect 3000 NMR spectrometer and 500 MHz Agilent VNMRS Nuclear Magnetic Resonance Spectrometer (Figure 3.9) with deuterated dimethyl sulphoxide, DMSO as a solvent. Values were recorded as ppm relative to internal standard (TMS).

Figure 3.9: Agilent VNMRS 500 MHz Nuclear Magnetic Resonance Spectrometer.

- Viscosity average (M_v) molecular weight of P(AN-co-VAc) was determined in DMF solvent using Ubbelohde equipment. The intrinsic viscosity of the polymer solutions in DMF was determined by Ubbelodhe viscometer at 27.5 for P(AN-co-VAc). The molecular weight was calculated for P(AN-co-VAc) by the Mark–Houwink equations $[\eta] = K \times M_v^{\alpha}$, $K = 2.78 \times 10^{-4}$, $\alpha = 0.75$ [174]. Specific viscosities of P(AN-co-VAc) and P(AN-co-VAc) were calculated by the Ubbelohde viscometer.
- The DSC measurements were carried out on TA Q1000 DSC instrument DSC (Figure 3.10). The measurements of polymers were operated with 4 cycles. First cycle was heating from -20°C to 250°C, second cycle was cooling from 250°C to -20°C, third cycle was heating from -20°C to 250°C and fourth cycle was heating from -250°C to -30°C under N_2 atmosphere. Third cycles were considered for DSC analysis. Each sample was scanned at a heating rate of 10 °C min^{-1}.

Figure 3.10: TA Q1000 DSC instrument.

- Latex particles and resulting fibers were also characterized as morphological by Scanning Electron Microscope (two diffrent SEM devices are used, Gemini Leo Supra 35 VP and Carl Zeiss EVO MA 10) and by Atomic Force Microscope(Nanosurf EasyScan2 STM, Figure 3.11). The samples for the SEM measurements are prepared by coating of gold (Ion Sputter Metal Coating Device, MCM-100).

Figure 3.11: Nanosurf EasyScan2 AFM.

- Thermal and mechanical properties of molded films obtained by polymer composites were measured by using a TA Q800 Dynamic Mechanical Analyser, DMA (Figure 3.12). Thermal measurements of polymeric films were operated by multi- frequency-strain test method. Samples were heated from the ambient temperature to 150 ^{o}C by a heating rate of 3 ^{o}C/min with an applied frequency of 1 Hz. Mechanical measurements were operated by DMA controlled-force test method. The size of the P(AN-co-VAc)@PPy_1 film is 10.70 mm, 4.52 mm, 0.054 mm as length, width, thickness respectively. The size of the P(AN-co-VAc)@PPy_2 film is 11.00 mm, 5.40 mm, 0.055 mm as length, width, thickness respectively. The size of the P(AN-co-VAc)@PPy_3 film is 12.00 mm, 5.40 mm, 0.061 mm as length, width, thickness respectively. The size of the P(AN-co-VAc)@PPy_4 film is 14.94 mm, 5.85 mm, 0.055 mm as length, width, thickness respectively.

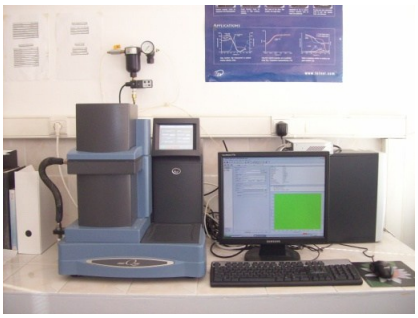

Figure 3.12: TA Q800 Dynamic Mechanical Analyser.

- UV analysis of P(AN-co-VAc)@PPy_1, P(AN-co-VAc)@PPy_2, P(AN-co-VAc)@PPy_3, P(AN-co-VAc)@PPy_4 nanofibers that were dissolved in DMF solvent, were carried out with UV-Visible Spectrophotometer (Perkin Elmer UV Visible Spectrophotometer, Figure 3.13).

Figure 3.13: Perkin Elmer UV Visible Spectrophotometer.

- Conductivity of electrospinning solution was measured with Parstat 2263 Electrochemical Analyser via EIS measurement (Figure 3.14). For the measurement, solutions that had 0.01 wt % polymer in DMF solvent were prepared. Three-electrode system consist of two platinum as working and counter and one silver as working electrode was used. Electrochemical impedance software named PowerSine was used to carry out impedance measurements between 10 Hz and 100 kHz.

Figure 3.14: Parstat 2263 Electrochemical Analyser.

4. RESULTS AND DISCUSSION

4.1 Copolymer and Composite Characterization

4.1.1 FTIR-ATR spectrophotometric analysis

The FTIR-ATR spectra of P(AN-co-VAc) and P(AN-co-VAc)/PPy are shown in Figure 4.1 and it was recorded in the absorbance mode.

PAN shows its characteristic absorption peaks at 2243 cm^{-1} and 1451 cm^{-1}, corresponding to CN stretching and CH bending, respectively. The C=O stretching, C-O-C stretching and C-O stretching vibration peaks can be observed at 1736, 1232, and 1022 cm^{-1}, respectively for PVAc. The strong absorption bands for P(AN-co-VAc) are C=O stretching (1736 cm^{-1}) and CN stretching (2243 cm^{-1}). These results are in agreement with literature [156,157].

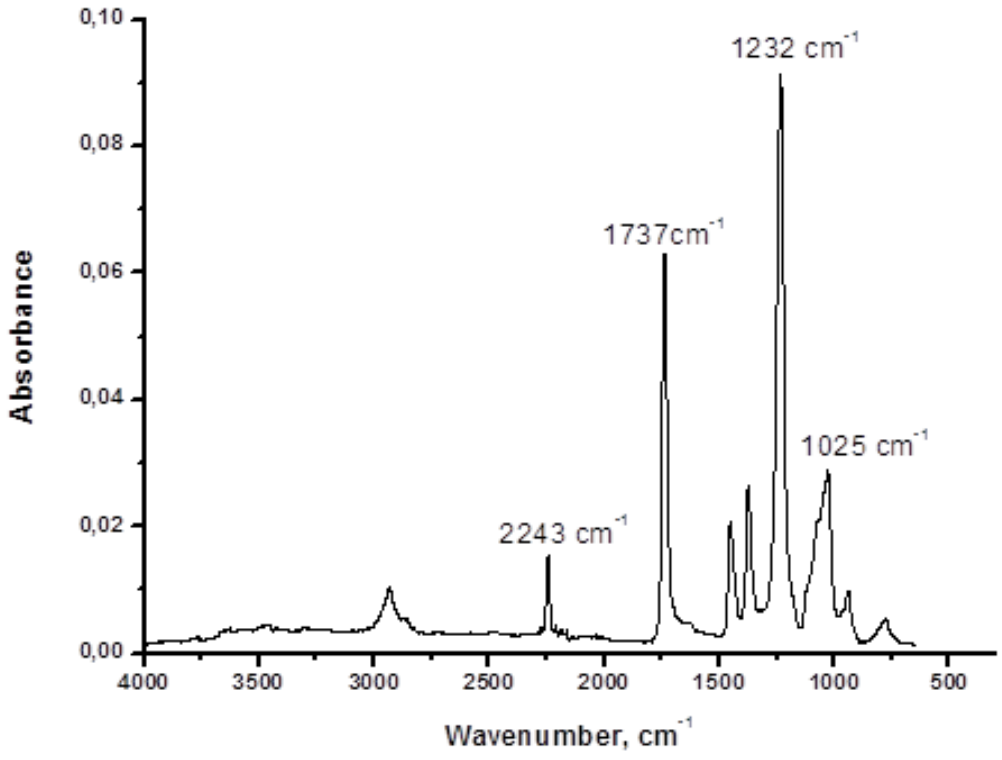

Figure 4.1: FTIR-ATR spectra of powder form of P(AN-co-VAc).

Figure 4.2 shows the FTIR-ATR spectrums of nanofibers that prepared 10 wt.% DMF solution. According to the this graph, FTIR-ATR spectrums for both of them approximately are the same except the characteristic peak of DMF at 1666 cm^{-1} due to the C=O stretching mode.

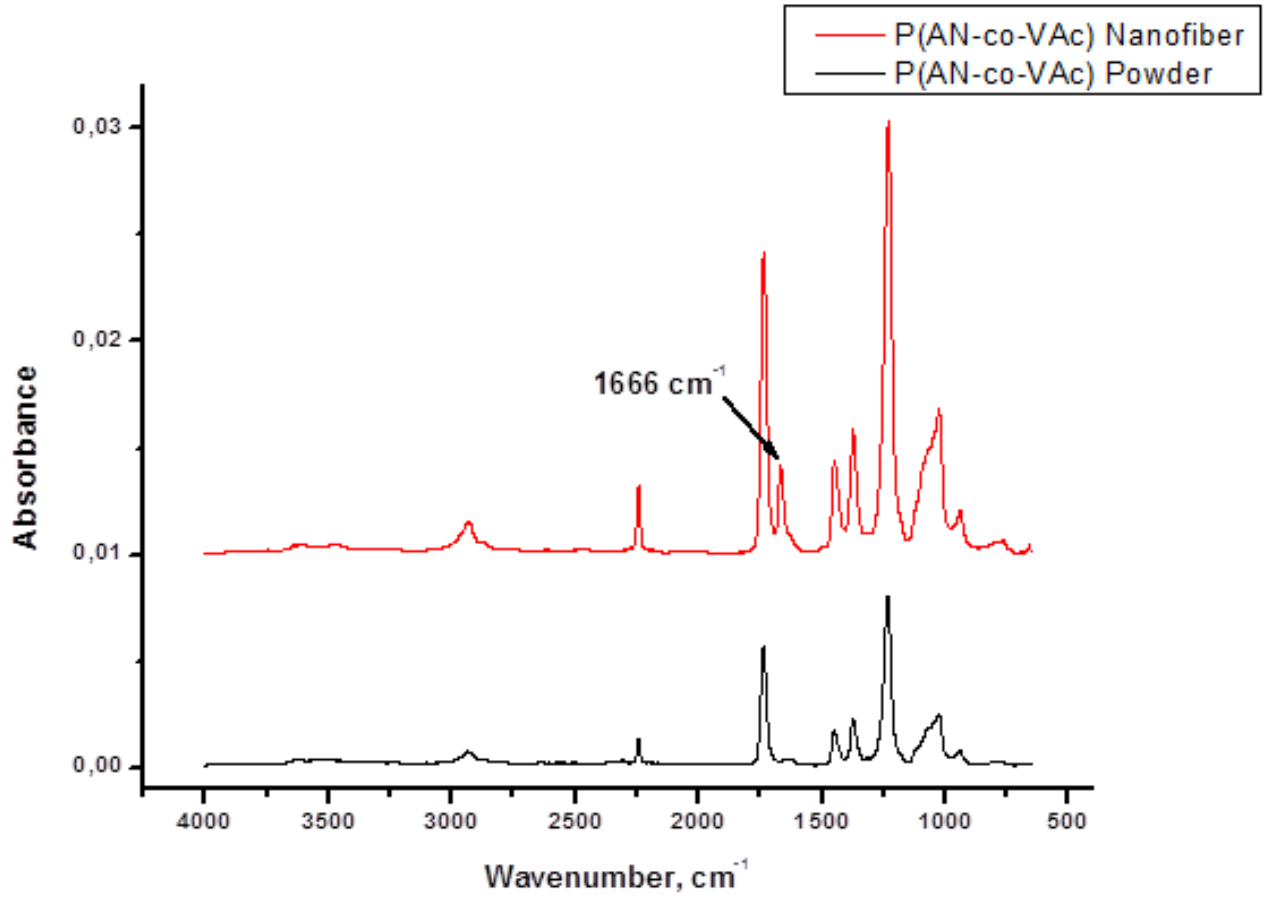

Figure 4.2: FTIR-ATR spectra of prepared P(AN-co-VAc) nanofibers (red line), and P(AN-co-VAc) in powder form (black line).

The P(AN-co-VAc) copolymer and composites of P(AN-co-VAc)/PPy in powder form were characterized by FTIR-ATR spectrophotometer and the change of Py was investigated depending on the changes in the absorbance values of PPy characteristic C-N stretching peak at 1451cm^{-1}. FTIR-ATR spectrums of P(AN-co-VAc) copolymer and composites of P(AN-co-VAc)/PPy were shown in Figure 4.5. PPy in the P(AN-co-VAc)/PPy composites was weak to show its characteristic band due to the presence of P(AN-co-VAc) backbone that was represented in Figure 4.4.

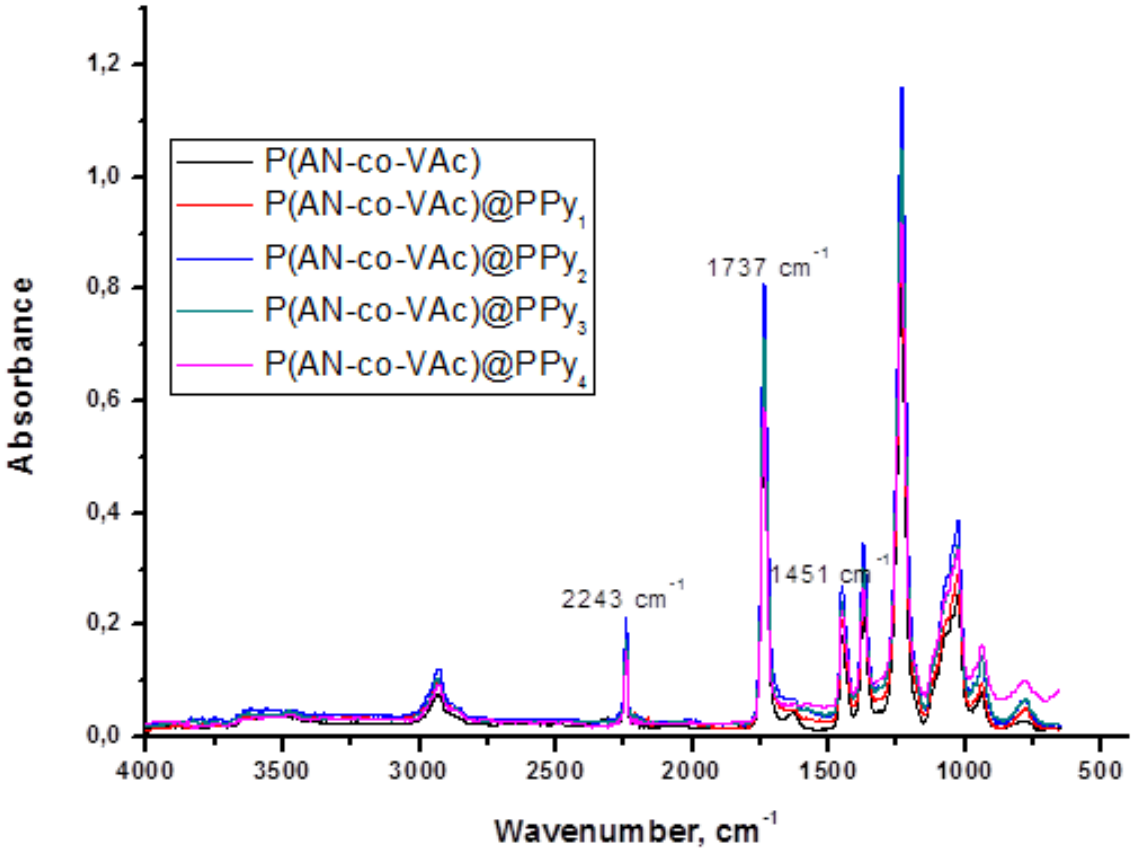

Figure 4.3: FTIR-ATR spectra of P(AN-co-VAc) copolymer and composites of P(AN-co-VAc)/PPy.

Approximately same stretching frequencies observed in the FTIR for P(AN-co-VAc) as well as for P(AN-co-VAc)/PPy composites. Due to the coinciding of peaks, FTIR might have not given different stretching frequencies in the composite. Therefore, as FTIR did not show much variation in their stretching frequencies for the P(AN-co-VAc) and P(AN-co-VAc)/PPy composite, it implies weak interaction due to the low content of PPy and more ordered arrangement of the copolymer and the composite [158].

PPy has interactions with nitrile (CN) and carbonyl (C=O) groups of P(AN-co-VAc) as a result of chemical polymerization. The nitrile (CN) groups and especially carbonyl (C=O) groups play a significant role on the interactions between those segments (C=O and CN) and PPy cationic sites [159].Thus, increase in CN absorbance band at 1451 cm^{-1} corresponding to the increase in Py feed ratio was observed.

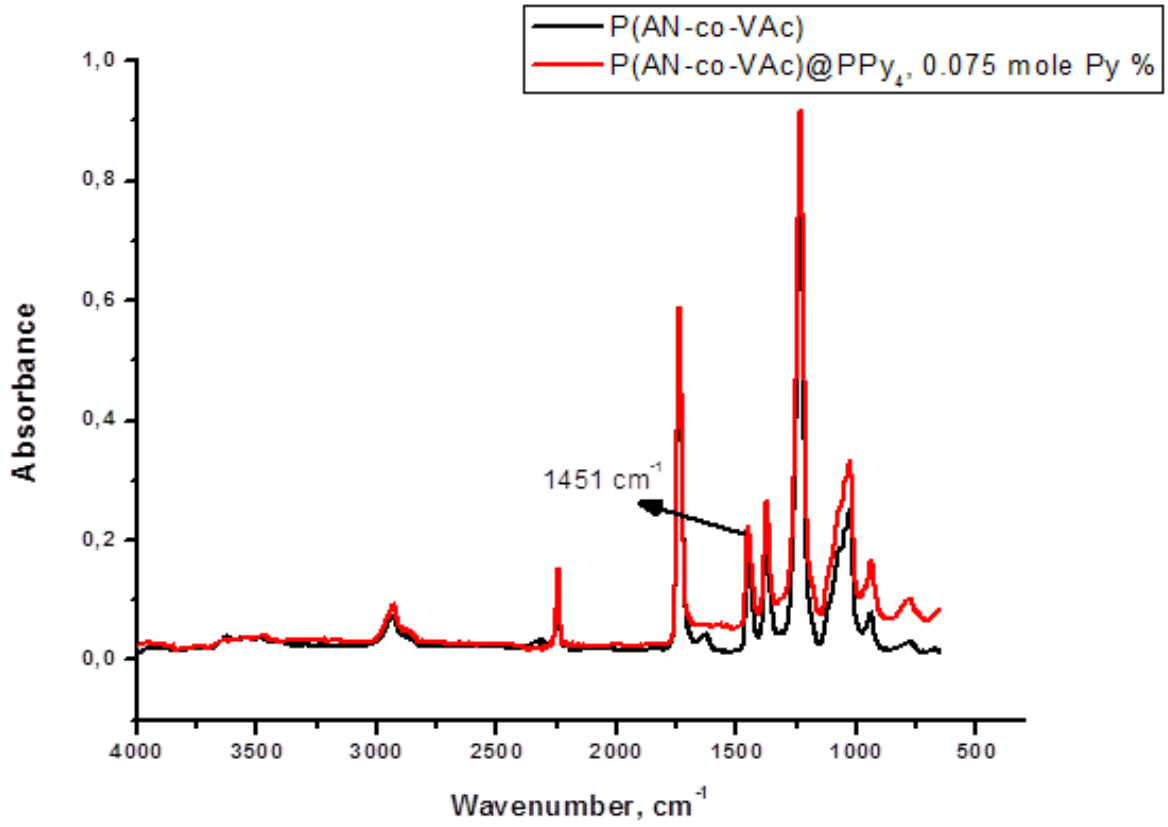

Figure 4.4: FTIR-ATR spectra of P(AN-co-VAc) copolymer and composites of P(AN-co-VAc)/PPy4, Py feeding ratio of 0.075 mole %.

4.1.2 Nuclear magnetic resonance (NMR) spectroscopy of P(AN-co-VAc) and P(AN-co-VAc)/PPy

^{1}H NMR spectrums of copolymer was obtained by using a 250 MHz Bruker AC Aspect 3000 NMR spectrometer. Figure 4.5 shows the ^{1}H-NMR spectra of copolymer recorded in Deuterated dimethyl sulphoxide (DMSO) using TMS as the internal standard.

The peak at δ=2.07 ppm is related to –CH_2 protons of both AN and VAc and the peak at δ=3.12 ppm is due to –CH proton of AN. Observing other peak δ=5.13 ppm due to –CH proton of VAc. These peaks are in agreement with literature [160]. The mole fraction of P(AN-co-VAc) was calculated from the ratio of the peak areas 5.13 ppm, corresponding to total peak area of 5.13 and 3. 12. Mol fraction of copolymer, m/(m+n) was calculated as 0.284.

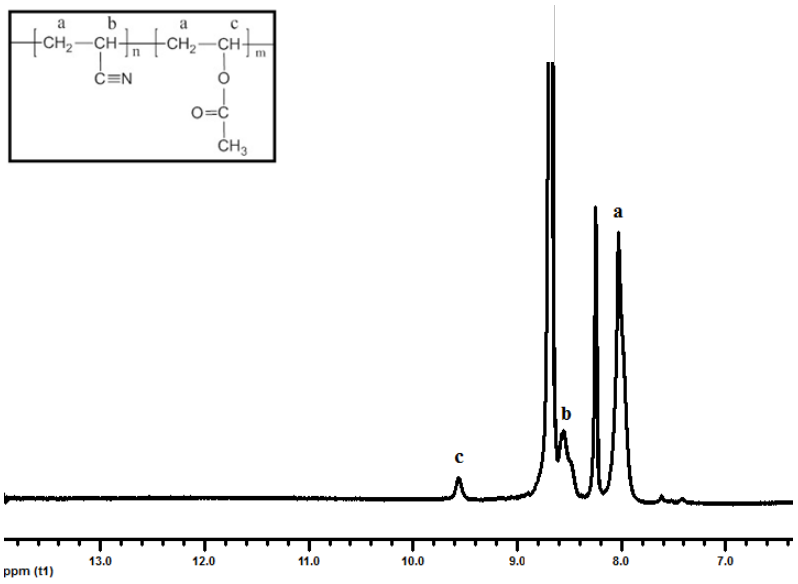

Figure 4.5: NMR spectrum of P(AN-co-VAc).

NMR spectrum (Figure 4.6) of P(AN-co-VAc)/PPy dissolved in DMSO solution displays a new peaks at 8.0–8.1 which is assigned to hydrogens in PPy rings [161]. It is well known that pure PPY is insoluble in DMSO, while P(AN-co-VAc)/PPy polymer can be dissolved in several organic solvents such as DMF and DMSO. The solution behavior of P(AN-co- VAc)/PPy as same as that of P(AN-co-VAc) confirms further the successful addition of PPy onto P(AN-co-VAc) by using DBSA as surfactant but also as dopant which creates increase in the solubility of PPy [65].

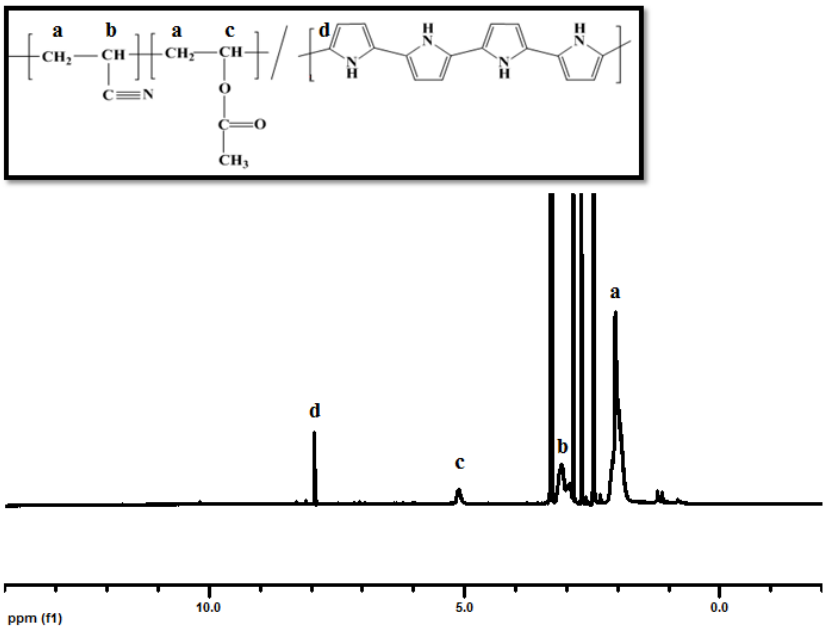

Figure 4.6: NMR Spectrum of P(AN-co-VAc)@PPy_4

4.1.3 UV- Visible spectrophotometric analyses

Dissolved nanofibers in DMF were analysed by UV-visible spectrophotometer (Figure 4.8). Nanofiber solution concentration was 0.11 wt % and kept constant for every measurements of composites. UV-Vis spectroscopy of polypyrrole shows an absorbance maxima at about 430 in figure 4.7. This peak has been attributed to transitions of the valence to polaron and bipolaron/polaron states. A broad absorption peak that was observed between 550 nm and 900 nm, is related to PPy. In spite of the π-π* transition of pyrrole units, these absorption peaks were obtained [162].

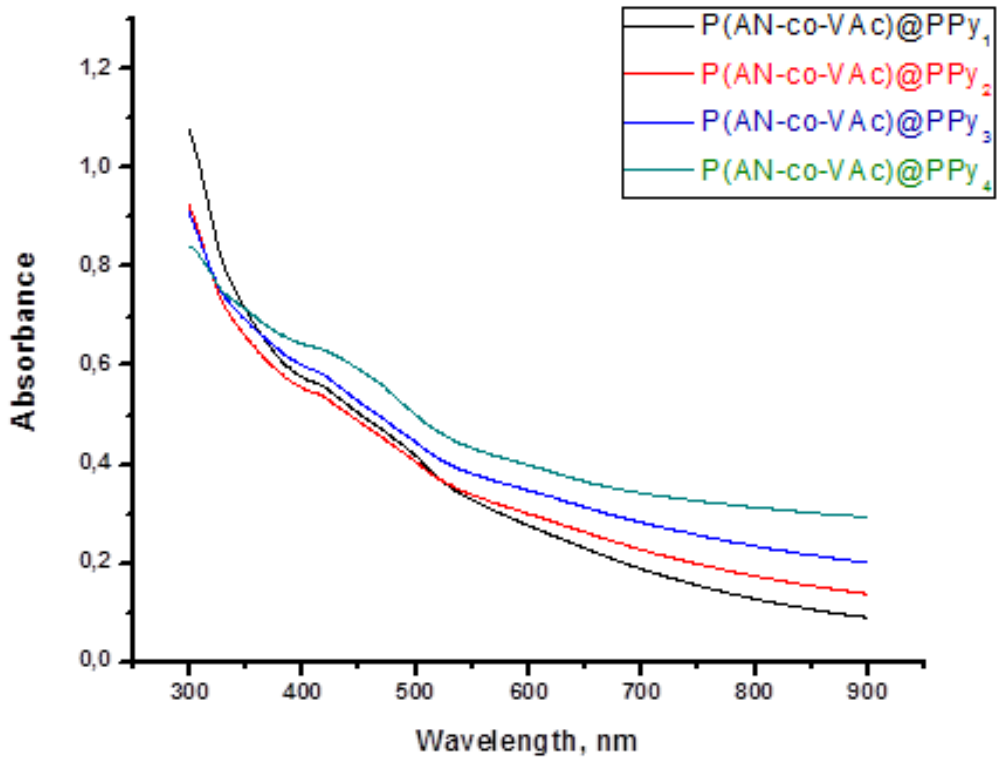

Figure 4.7: UV-Vis Spectrum of P(AN-co-VAc)@PPy$_{1,}$ P(AN-co-VAc)@PPy$_{2,}$ P(AN-co-VAc)@PPy$_{3,}$ P(AN-co-VAc)@PPy$_{4.}$

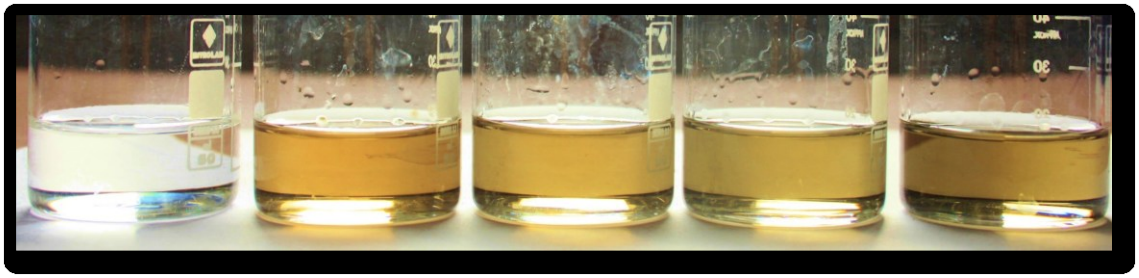

Figure 4.8: Dissolved nanofibers of P(AN-co-VAc), P(AN-co-VAc)@PPy$_{1,}$ P(AN-co-VAc)@PPy$_{2,}$ P(AN-co-VAc)@PPy$_{3,}$ P(AN-co-VAc)@PPy$_{4.}$

Relationship between, FTIR-ATR and UV-Vis results were shown in the figure 4.9. C-N stretching peak of PPy shows its characteristic peak at 1451cm^{-1}, which result is in agreement with literature [163].

An increase in the FTIR absorbance values of PPy at 1451 cm^{-1} was observed corresponding to PPy wt% feed ratio and also same trend was occurred in the UV-Vis measurement due to incease in the maximum point of the peak at 430 nm related to Py characteristic peak at UV-Vis spectrum. Correlation of these results depicted in Figure 4.9.

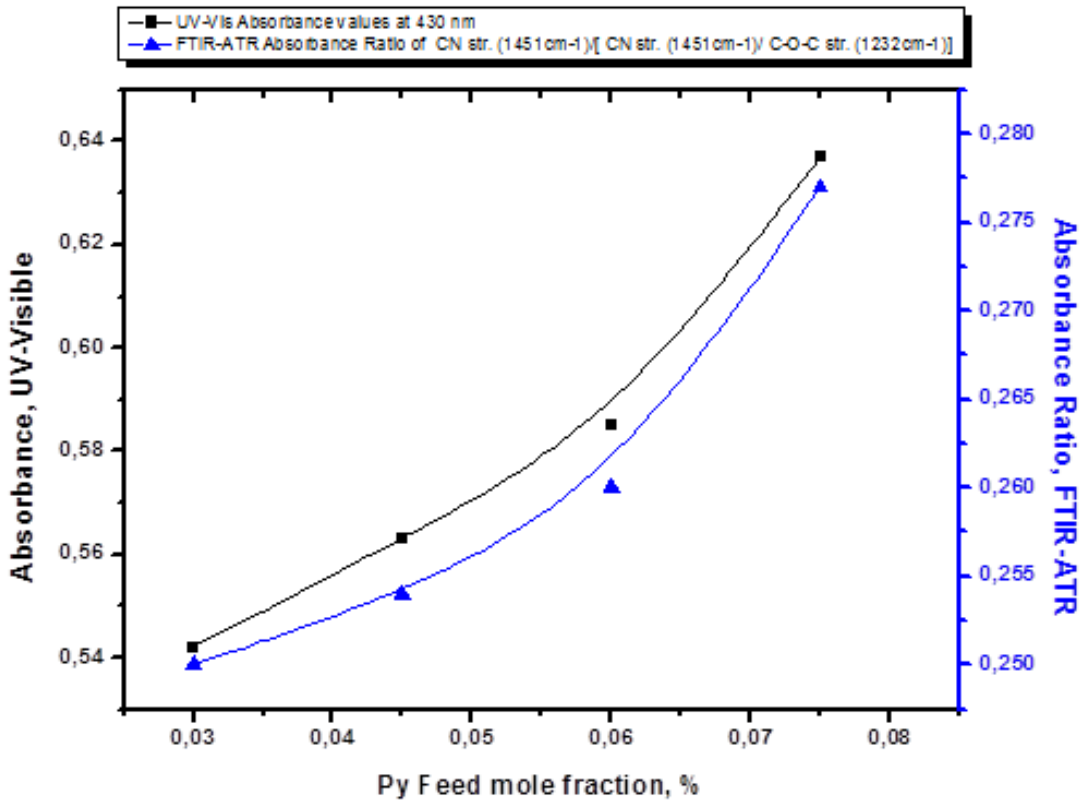

Figure 4.9: Correlation between FTIR-ATR absorbance ratio of CN str. (1451cm^{-1})/[CN str. (1451cm^{-1})/ C-O-C str. (1232cm^{-1})], UV-Vis absorbance values at 430 nm and Py feed mole fraction.

4.1.4 Differential scanning calorimetry measurement (DSC) of P(AN-co-VAc) and P(AN-co-VAc)/PPy composites

T_g values of the P(AN-co-VAc) and P(AN-co-VAc)@PPy$_1$, P(AN-co-VAc)@PPy$_2$ were determined as 97.09 °C, 99.03 °C and 99.67 °C (Figure 4.10), respectively and

it is realized that the presence of the PPy content in the copolymers caused a increase in the T_g values due to the decrease in chain flexibility.

T_g value of PPy homopolymer was reported as around 120 ^oC [164] and PAN homopolymer had a T_g of 210 ^oC. It was also reported that T_g value of poly(AN-co-VAc) random copolymer dropped T_g to 92.5^oC [165].

According to the literature, the considerable steric hinderance and stiffness of the side PPy chains will depress the P(ANco-VAc)/PPy main chain segments mobility and raise the T_g. Increasing trend of T_g value with Py content is due to decrease in main chain flexibility. These results are in agreement with the literature [166].

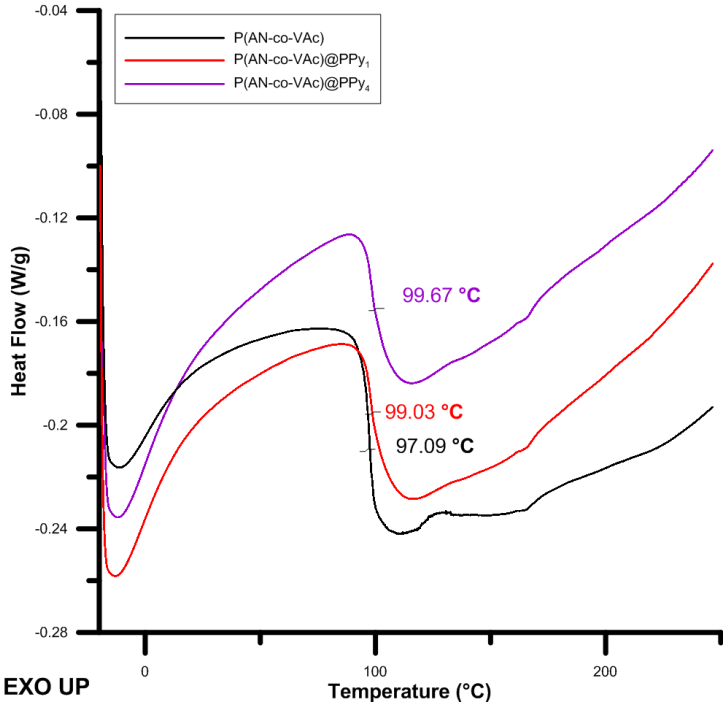

Figure 4.10: DSC graph of P(AN-co-VAc), P(AN-co-VAc)@PPy$_1$, P(AN-co-VAc)PPy$_4$.

4.1.5 T_g Determination by DMA

The DMA gives information about glass transition (T_g) and viscoelastic properties of polymeric amorphous materials. Under tension/compression deformations the measured viscous component is referred to as the loss modulus (E”), while the measured elastic component is referred to as the storage modulus (E’). The ratio of the loss modulus to the storage modulus is referred to as the loss tangent (E”/E’), or tan delta [167]. T_g of the composites is located as the temperature where tan delta is maximum (Figure 4.11).

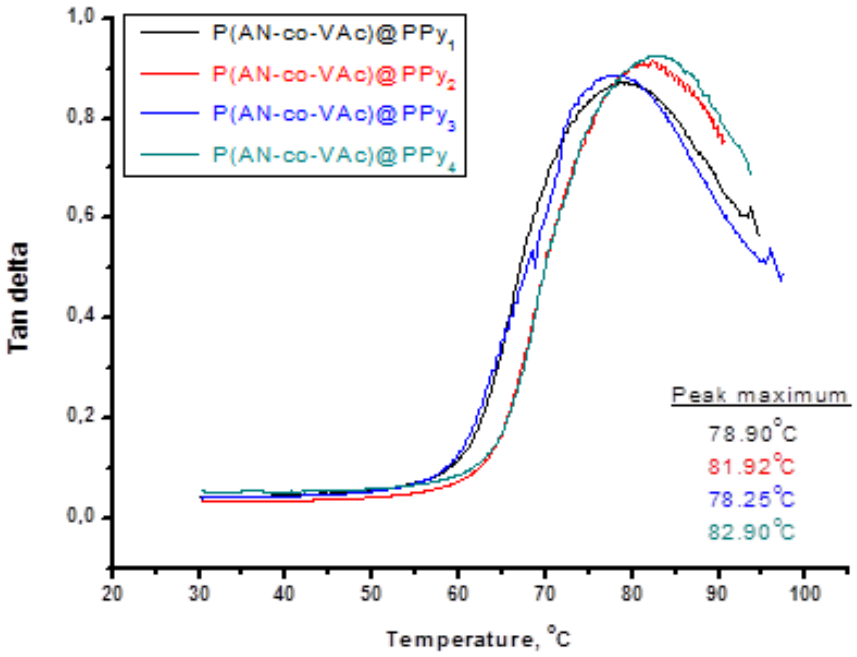

Figure 4.11: T_g values of composites obtained by DMA.

T_g values of the P(AN-co-VAc) and P(AN-co-VAc)@PPy_1, P(AN-co-VAc)@PPy_2, P(AN-co-VAc)@PPy_3, P(AN-co-VAc)@PPy_4 were determined as 78.90 °C, 81.92 °C, 78.25 °C and 82.90 °C respectively and the presence of the PPy content in the copolymers caused same trend with DSC analysis results. Correlation between Tg values obtained from DSC and DMA corresponding to Py feed mole fraction (mole %) was given in the figure 4.12.

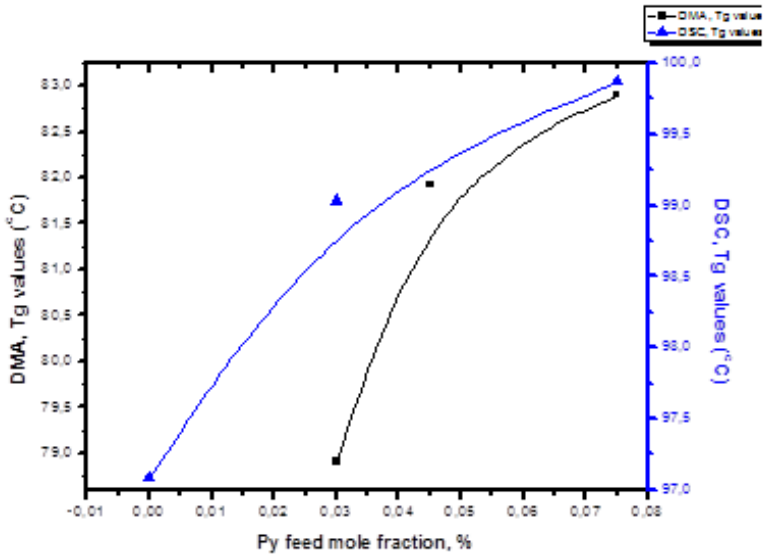

Figure 4.12: Correlation between Tg values obtained from DSC and DMA corresponding to Py feed mole fraction (mole %).

4.1.6 Viscosity and molecular weight determination

The intrinsic viscosity of the polymer solutions in DMF was determined by Ubbelodhe viscometer at 28 ^{o}C for P(AN-co-VAc) by DMF as a solvent. The molecular weight was calculated for P(AN-co-VAc) copolymer of 30 wt % VAc feed ratio were calculated as 380,190 g/mole due to the intercept value that is called as intrinsic viscocity in figure 4.13 by using Mark–Houwink equation.

Specific viscosities of P(AN-co-VAc) and P(AN-co-VAc)/PPy obtained from Ubbelohde type viscometer at 28 ^{o}C are given in Table 4.1.

Table 4.1: P(AN-co-VAc), P(AN-co-VAc)/PPy specific viscosity results.

	P(AN-co-VAc)	P(AN-co-VAc)PPy_1	P(AN-co-VAc)PPy_2	P(AN-co-VAc)@PPy_3	P(AN-co-VAc)@PPy_4
η_s	0.32632	0,15789	0.14737	0.09474	0.08421

In spite of the increase pyrrole feed ratio, a reduction in specific viscosities were determined. Low viscosity as a result of the low molecular weight of conductive polymers [168].

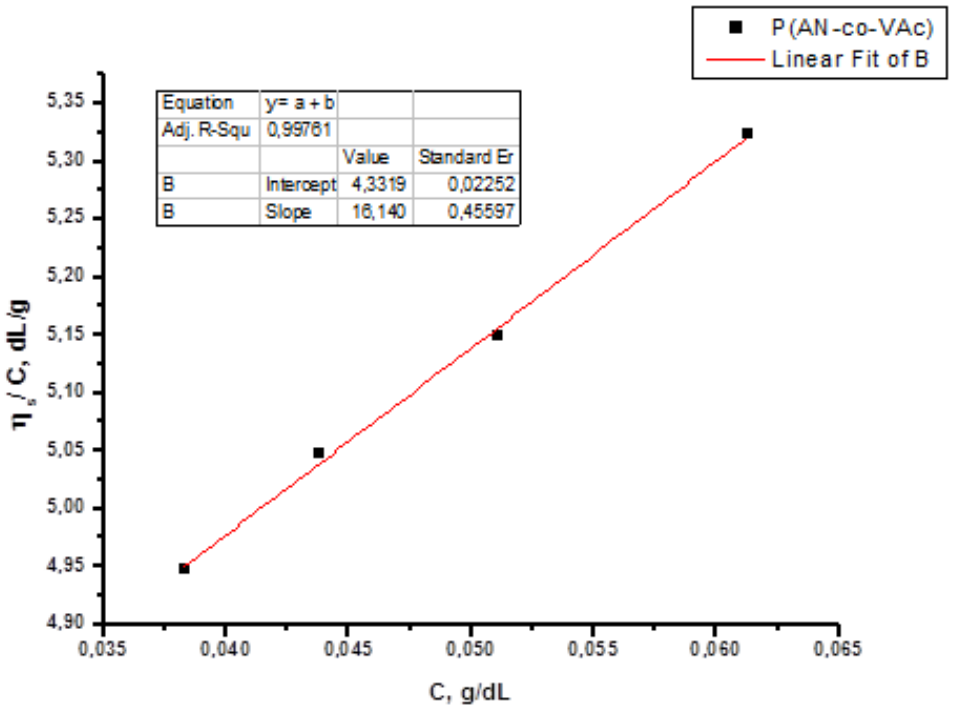

Figure 4.13: The intrinsic viscosity calibration curve (η_s/C versus C).

4.1.7 Particle size measurements, SEM

Latex form of P(AN-co-VAc) and P(AN-co-VAc)/PPy composites were used to investigate the particle's morphological properties. Effect of pyrrole addition in the composite synthesis was analysed.

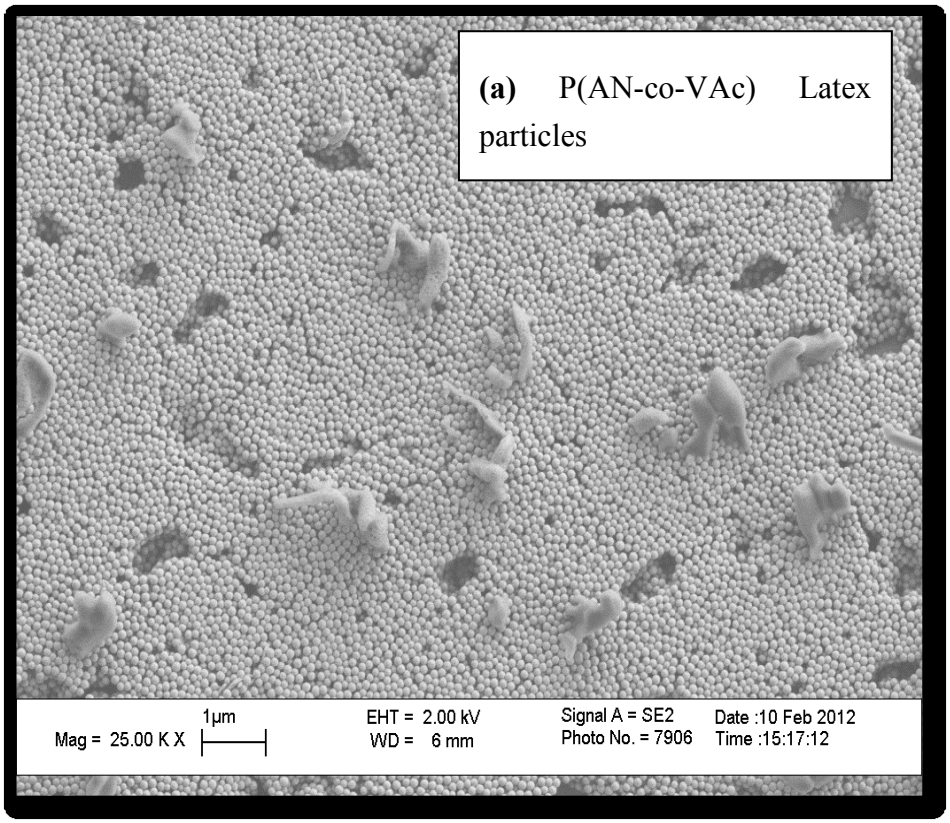

(a) P(AN-co-VAc) Latex particles

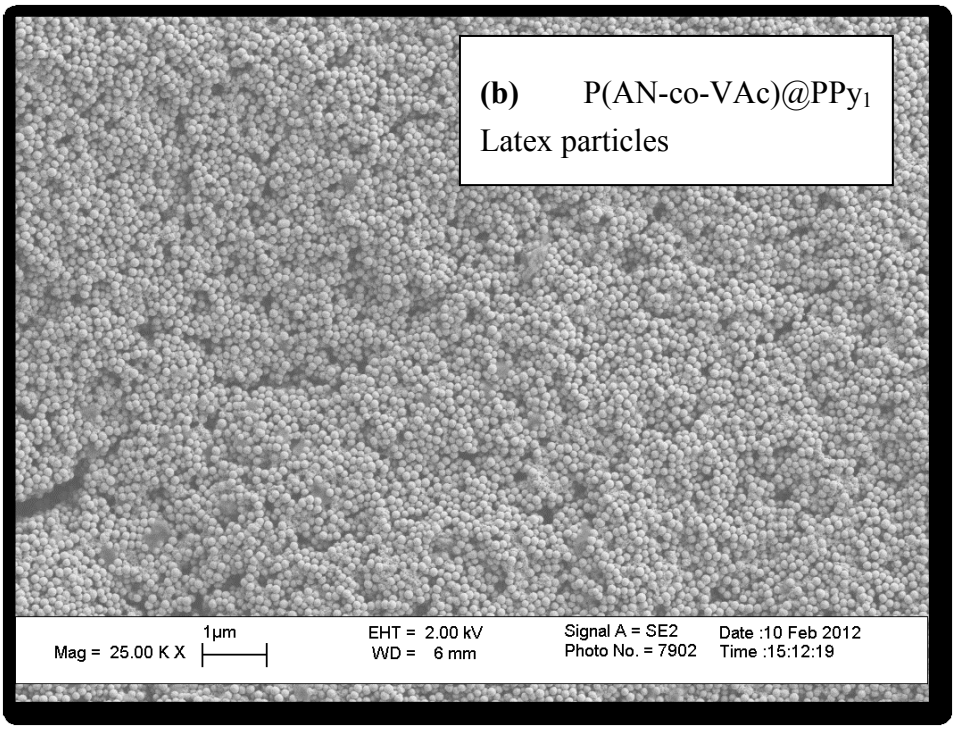

(b) P(AN-co-VAc)@PPy_1 Latex particles

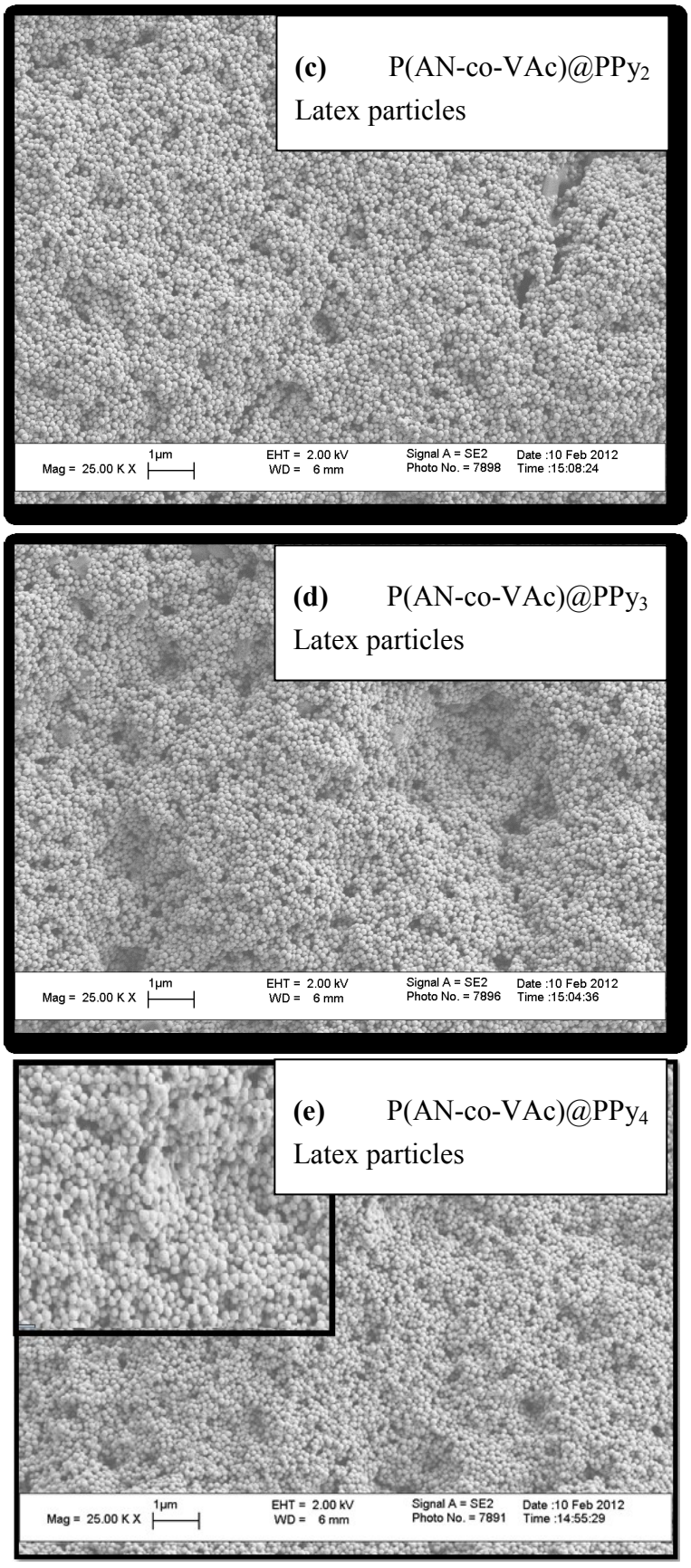

Figure 4.14: SEM images of latex particles of copolymer (a) and composites including different pyrrole content (b), (c), (d), (e).

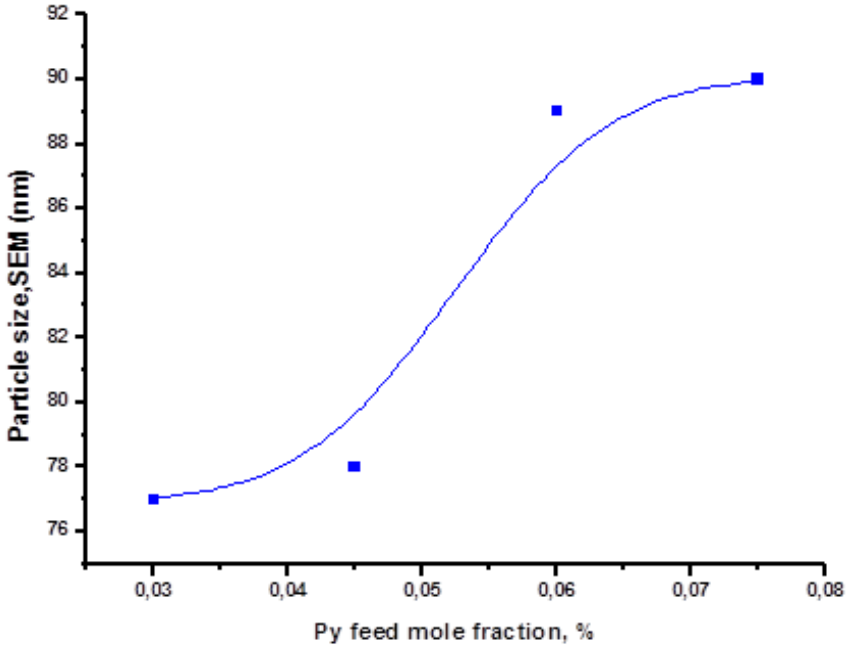

Figure 4.15 : Relation between Py content and size of latex particles in composites.

4.1.8 Dynamic mechanical analysis of composites

The slope of the stress-strain curve in the elastic deformation region is the modulus of elasticity, which is known as Young's modulus (elastic modulus). It represents the stiffness of the material-resistance to elastic strain.

The elastic modulus measurements of composites are reported in figure 4.16. Five specimens were tested for mechanical properties.. P(AN-co-VAc)/PPy composites showed brittle mechanical property. A decrease in tensile strength was observed for each composition in comparison to the P(AN-co-VAc) copolymer and tensile strength is decreasing with increasing pyrrole content in the composition.

Table 4.2: Toughness of polymers were shown in the table.

Sample	Toughness (N/mm^2)
P(AN-co-VAc) @PPy_1	0.624
P(AN-co-VAc) @PPy_2	0.588
P(AN-co-VAc) @PPy_3	0.838
P(AN-co-VAc) @PPy_4	1.073

The area under the stress-strain curve is known as toughness, which represents the total strain energy per unit volume in the material induced by the applied stress.

It was seen that the toughness increases with increasing content of Py in the composites. Increase in toughness was indicated in Table 4.3.

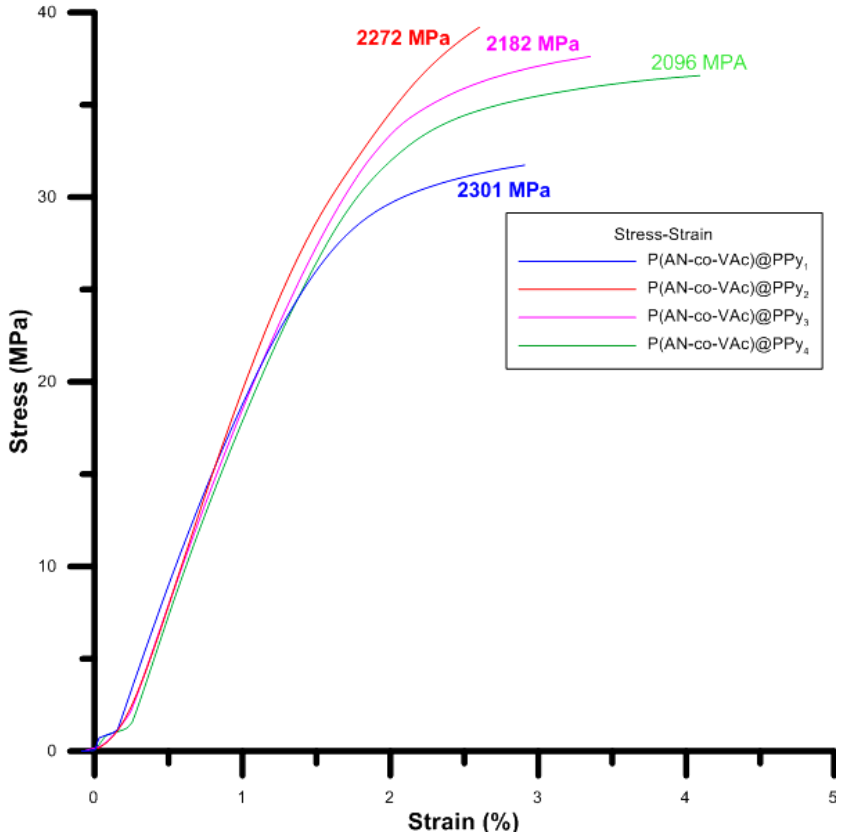

Figure 4.16: Stress-strain curve of polymers that were obtained by DMA.

4.1.9 Impedance spectroscopy measurements

The corresponding Admittance diagram was represented in figure 4.17. The analysis was conducted with 10mV ac amplitude at the open circuit potential (OCP), in the frequency range between 0.01 Hz and 100 kHz. The study is carried out in its own polymer solution. The curves corresponding to solutions of P(AN-co-VAc)@PPy_1, P(AN-co-VAc)@PPy_2, P(AN-co-VAc)@PPy_3 and P(AN-co-VAc showed an increase in conductivity with the increasing feed ratio of Py content.

Conductivity values were determined from Admittance diagrams. The lowest conductivity and the highest values are obtained from the formula of; Y=1/Z, where y and z are admittance and impedance. Due to this equation, solution of P(AN-co-VAc)'s conductivity was $6,7010^{-5}$ S, P(An-co-VAc)@PPy_1's conductivity was $3,25.10^{-4}$ S, P(An-co-VAc)@PPy_2's conductivity was $3,50.10^{-6}$ S, and P(An-co-VAc)@PPy_3's conductivity was calculated as $5,05.10^{-6}$ S.

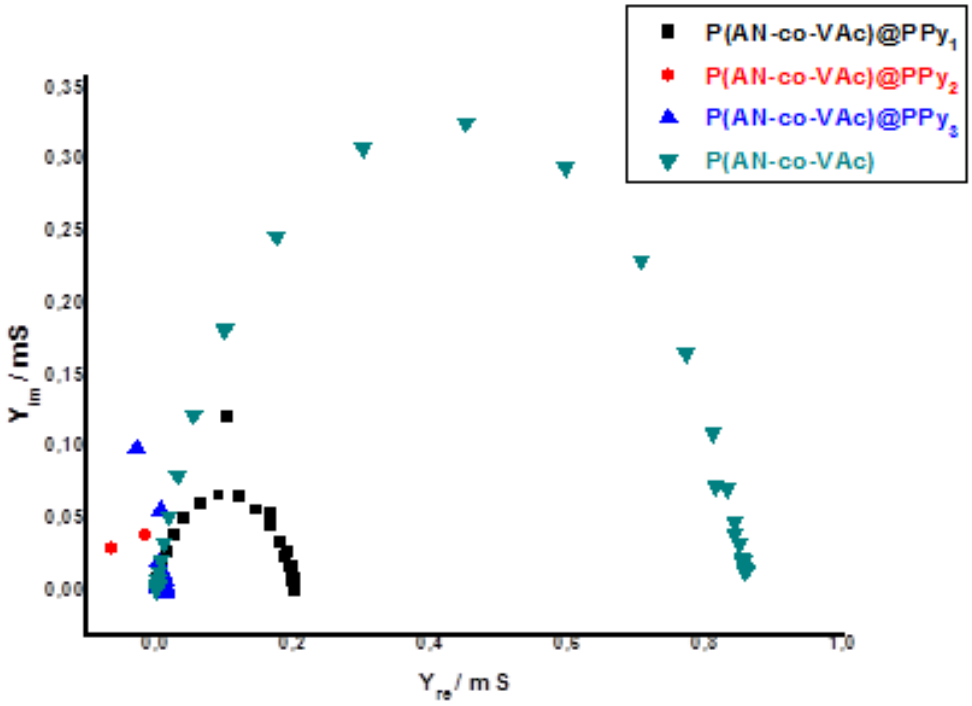

Figure 4.17: Admittance diagrams of P(AN-co-VAc)@PPy$_{1\text{-}2\text{-}3}$ solution in DMF and P(AN-co-VAc) in DMF solution.

4.2 Morhology of Fibers

The process of electrospinning P(AN-co-VAc) and P(AN-co-VAc)/PPy nanofibers is very stable and can be operated unattended for several hours to produce non-woven nanofiber mats. Morphologic properties of these polymers were shown in SEM and AFM images in figure 4.18 and 4.21. The average diameter of electrospun fibers of different concentrations is determined by using Imagej program to randomly measure the diameters of 40 individual fibers shown in SEM images with x20000 magnitude that was given in figure 4.18.

Mole percent of the initially added Py concentration varies from 0.030% to 0.075%. the average diameters of the nanofibers are reduced from 200 to 120 nm (Table 4.4). With the increase of the initially added Py concentrations, some beads begin to appear (Figures 4.18 (c) and (e)). This may be a result of the increased PPy content in the electrospinning solutions [169-171].

Bead-free nanofibers were obtained due to the greater polymer chain entanglements and viscosity of the solutions. Our method exhibited that PPy was homogeneously distributed in polymer composition and succesfully inclusion in to the copolymer.

The surface roughness due to the PPy on the nanofiber structure was obtained in previous studies. That morphological approach was related to PPy in the structure[163].

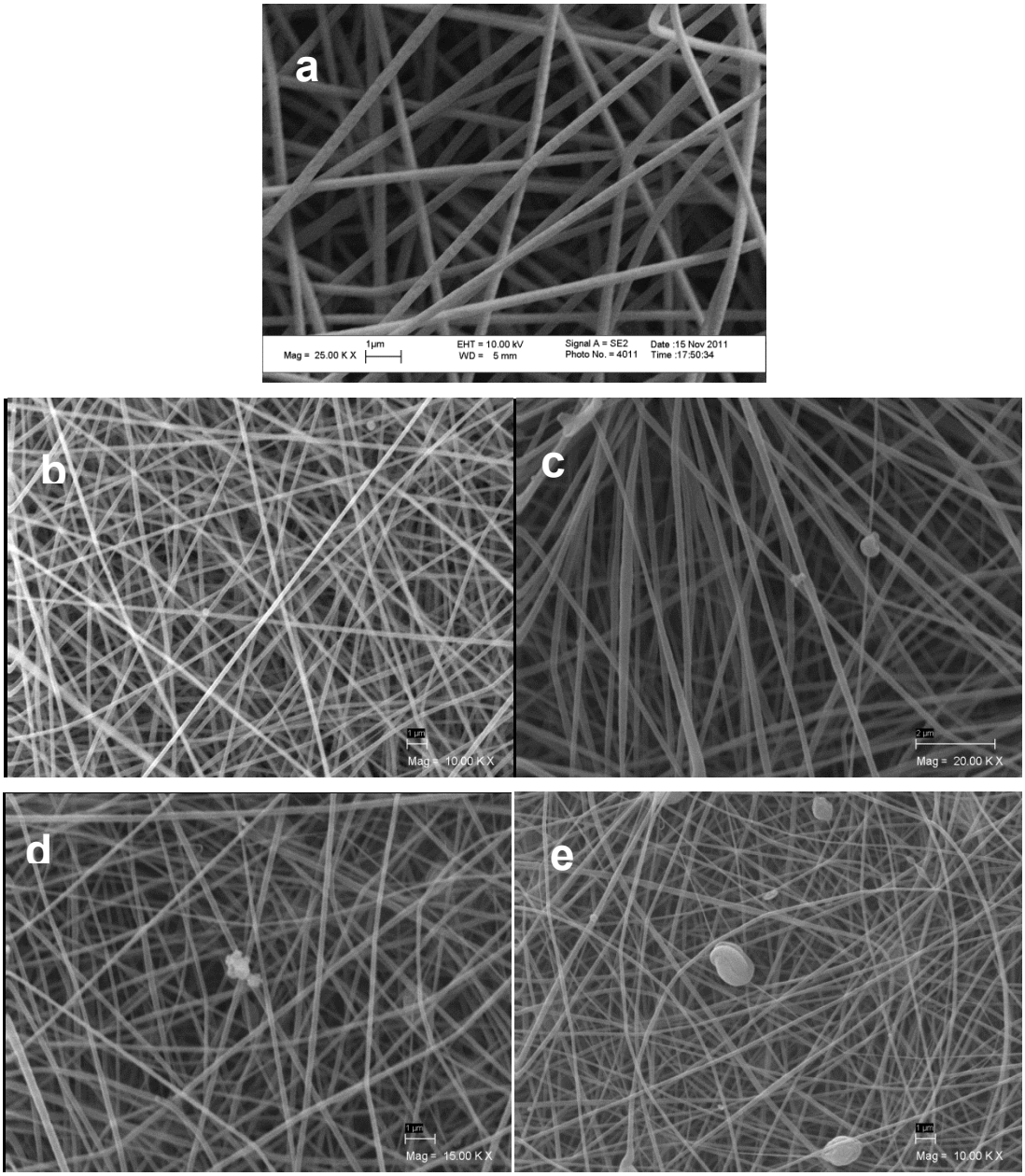

Figure 4.18: SEM images of P(AN-co-VAc)(a) and the samples at different PPy content: P(AN-co-VAc)@PPy_1, 0.030 mole % (b), P(AN-co-VAc)@PPy_2 , 0.045 mole % (c), P(AN-co-VAc)@PPy_3 , 0.060 mole % (d) and P(AN-co-VAc)@PPy_4 , 0.075 mole % (e).

In this study, elimination of surface roughness on nanofibers structure lead to dispersion of latex particles in composition and also improved solubility of PPy due to the effect of DBSA [65]. Photos of obtained nanofibers were given in figure 4.19.

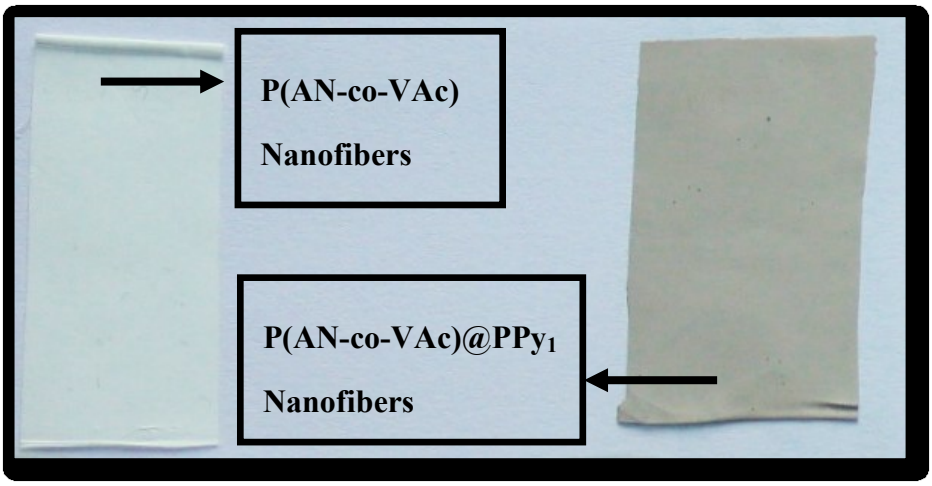

Figure 4.19: Photos of obtained nanofiber webs

Table 4.3: Standart deviation values and average nanofiber diameters.

	Py Feed Mole Fraction, %				
	-	**0.030**	**0.045**	**0.060**	**0.075**
Average fiber diameter, nm	310±24	200±11	170±21	125±26	120±25

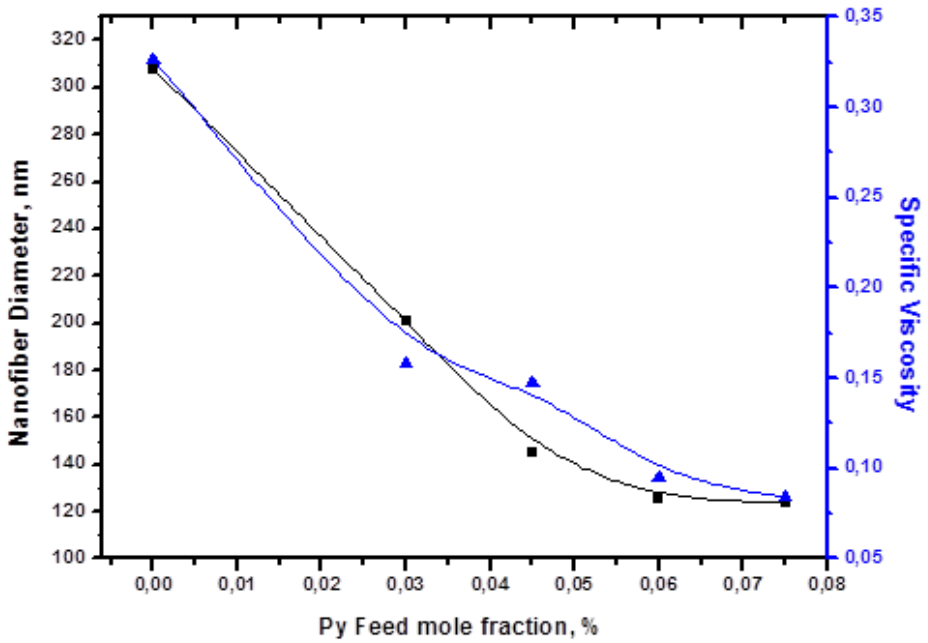

Figure 4.20: Relationship between nanofiber diameter, specific viscosity and Py feed mole fraction, %.

In figure 4.20, correlation between nanofiber diameters, viscosity and PPy feed ratio was examined. With the decrease of specific viscosity of polymers, low average nanofiber diameters were obtained. The low average nanofiber diameters probably result from the relatively low molecular weight of conductive polymers [172]. Therfore, PPy creates decrease in viscosity and that causes the smaller diameter of nanofibers. Moreover, Nanofibers have small average diameters related to the electropinning solutions that have higher conductivity [173].

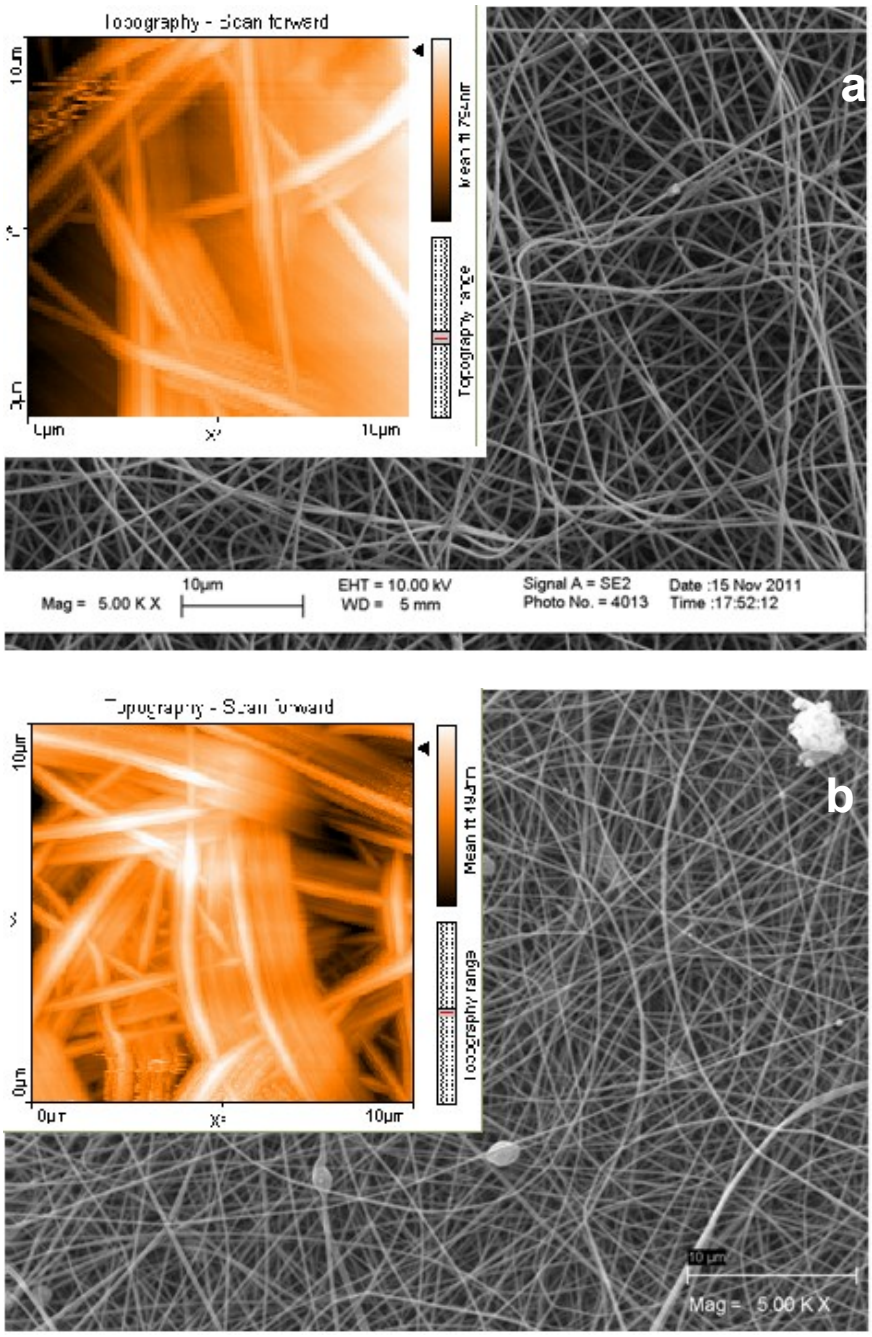

Figure 4.21: SEM and AFM images of P(AN-co-VAc) (a) and P(AN-co-VAc)@PPy$_4$ (b).

5. CONCLUSION

The first objective of this thesis was to obtain one step polymerized P(AN-co-VAc)/PPy composites. After that producing nanofibers from these composites were taken as a goal of this study by electrospinning method. Therefore, first acrylonitrile-vinyl acetate copolymer was synthesized [P(AN-co-VAc)] by Emulsion polymerization in aqeuos medium. Composites were obtained with continued polymerization during 18 hours with adding different quantity of pyrrole in 4 sample flasks and stirring and mixing throughout reaction time. FTIR-ATR spectra and NMR spectrum of copolymer revealed that AN and VAc had effectively participated in polymerization and also FTIR-ATR, UV-Vis spectra and especially NMR spectrum of P(AN-co-VAc)/PPy composites showed that Py had participated in polymerization. SEM images indicated the morphology of latex particles. Participation of PPy to the copolymer latex particles were obviously observed. By DSC and DMA, thermal effect of PPy on the copolymer structure was investigated. Increase in glass transition temperatures with increasing feed pyrrole ratio were lead to lack of chain flexibility of polymer. DMA also revealled that the brittleness of PPy caused decrease in tensile strength of polymer films.While making comparison with nanofiber diameters of P(AN-co-VAc) copolymer and P(AN-co-VAc)/PPy composites. It was clearly seen that nanofiber diameters were strongly dependent on pyrrole content in composites. Due to the improvement in PPy solubility with the effect of DBSA, smoother and more homogeneus fiber morphology were obtained. Mole percent of the initially added Py concentration varies from 0.030% to 0.075%, the average diameters of the nanofibers were reduced from 200 to 120 nm. The diameters of the fibers decrease slightly with the increase of Py feed ratio in composition. With the increase of the initially added Py concentrations, some beads begin to appear. Therefore, this may be a result of the increased PPy content in the electrospinning solutions and also decrease in viscosity.

REFERENCES

[1] R. Gangopadhyay, A. De, (2000). Chem. Mater. 12, 608

[2] T. Zhang, Y. He, R. Wang, W. Geng, Sens. (2008). Actuators B 131, 687

[3] K. Majid, R. Tabassum, A.F. Shah, S. Ahmad, M.L. Singla, (2009). J Mater. Sci. Mater. Electron. 20, 958

[4] S. Xing, G. Zhao, (2006). Polym. Bull. 57, 933

[5] N. Kizilyar, L. Toppare, A. O¨ nen, Y. Yagci, (1998). Polym. Bull. 40, 639

[6] K. Ishiyama, K. Imamura, K.I. Arai, J. (2002). Magn. Mater. 242, 1163

[7] C. Smyth, K.T. Lau, R.L. Shepherd, D. Diamond, Y. Wu, G.M. Spinks, G.G. Wallace, (2008). Sens. Actuators B. 129, 518

[8] T. Yao, C. Wang, J. Wu, Q. Lin, K. Zhang, J. (2009). Colloid. Interf. Sci. 338, 573

[9] H. Koezuka, A. Tsumura, (1989). Synth. Met. 28, 753

[10] J. Gao, H. Heegar, J.Y. Lee, C.Y. Kim, (1996). Synth. Met. 82, 221

[11] T.A. Skothein, R.L. Elsenbaumer, J.R. Reynolds, (1998). Handbook of Conducting Polymer, 2nd edn. (Marcel Dekker, Inc., New York), p. 226

[12] P.B. Landon, J. Gutierrez, C.L. Gilleland, L. Jordan, (2007). J. Mater. Sci. Mater. Electron. 18, 235

[13] H. Chen, J. Chen, K.A. Liyan, H. Wenbo, L. Zhengping, Z. Qingyue, Chin. (2005)Sci. Bull. 50, 971

[14] Sahoo, N. G., Jung, Y. C., So, H. H., and Cho, J. W., (2007). Polypyrrole Coated Carbon Nanotubes: Synthesis, Characterization, and Enhanced Electrical Properties, *Synth. Met*., 157, 374–379

[15] Li, N., Shan, D., and Xue, H., (2007). Electrochemical Synthesis and Characterization of Poly(Pyrrole-co-Tetrahydrofuran) Conducting Copolymer, *Eur. Polym. J.*, 43, 2532–2539

[16] Zhang, Z., Roy, R., Dugre, F. J., Tessier, D., and Dao, L. H., (2001). In vitro Biocompatibility Study of Electrically Conductive Polypyrrole-coated Polyester Fabrics, *J. Biomed. Mater. Res.*, 57, 63–71

[17] Kaynak, A., and Beltran, R., (2003).Effect of Synthesis Parameters on the Electrical Conductivity of Polypyrrole-coated Poly(Ethylene Terephthalate) Fabrics, *Polym Int.*, 52, 1021–1026

[18] C.J. Thompson, C.J., Chase, G.G, Yarin, A.L., Reneker, D.H., (2007). Polymer 48, 6913-6922

[19] Ueda, W., Morooka, Y., and Sasaki, Y. (1992). Petrotech (Tokyo), 15: 346

[20] Monjol, P., and Champetier, G. (1972). Bull. Soc. Chim. Fr., 4: 1302.

[21] Quingling, C., Xin, C., Liansheng, M., and Wencai, C. (1999). Catal. Today, 51: 141.

[22] Peng, F. M. (1995). In Encyclopedia of Polymer Science and Engineering; Mark, H. F., Bikales, N. M., Overberger, C. G., Menges, G., Kroschwitz, J. I., Eds.; Wiley: New York, Vol. 1, p 426.

[23] Nuyken, O.; Lattermann, G. In *Handbook of Polymer Synthesis*; Kricheldorf, H. R., Ed.; Marcel Dekker: New York, 1992; Vol. 1, pp 223.

[24] Chae DW, Kim BC. (2006). Journal of Applied Polymer Science, 99:1854-1858.

[25] Landfester K, Antinietti M. Macromol. (2010). Rapid Commun;21:820-824.

[26] Bhanu VA, Rangarajan P, Wiles K, Bortner M, Sankarpandian M, Godshall D, Glass TE, Banthia AK, Yang J, Wilkes G, Baird D, McGrath JE. Polymer 2002;43:4841-4850

[27] Han N, Zhang XX, Wang XC. 2010 Iranian Polymer Journal;19:243-253

[28] Carraher, C. E., Seymour/Carraher's Polymer Chemistry, sixth edition, (2003), p.406, ISBN: 0–8247–0806–7

[29] Zhang C, Du Z, Li H, Ruckenstein E., (2002). Polymer;43:2945-2951

[30] Lia YH, Zhou DY, Rao MM, Li WS, Ca ZP, Liang Y, Tan CL, (2009). Journal of Power Sources, 189:139-144

[31] Qiu G, Tang ZL, Huang NX, Chen HJ. (2001). Journal of Applied Polymer Science, 82:854-860

[32] Moghadam SS, Bahrami SH., (2005). Iranian Polymer Journal;14:103-141.

[33] Reddy, G., V., R., Ranganathan, R., Sivakumar, S. And Sriram, r., (2002). Emulsion copolymerizations of methyl acrylate with methyl methacrylate and with acrylonitrile, Designed Monomers and Polymers, Vol. 5, No. 1, pp. 97–114

[34] Candau, F., (1989).Scientific Methods for the Study of Polymer Colloids and Their Applications, p.1, 1989

[35] El-Aasser, M.S. nad Fitch, R.M., (1987). In Future Directions in Polymer Colloids, Eds., NATO ASI, Series E, Applied Sciences No. 138; Nijhoff.

[36] Poehlein, G.W., Ottewill, R.H. and Goodwin, J.W., (1983). In science and Technology of Polymer Coloids, Eds. NATO ASI, Series E, Applied Sciences No.67

[37] Piirma, I., (1982). In Emulsion Polymerization, Academic Press, New York

[38] Bassett, D.R. and Hamielec, A.E., (1981). In Emulsion Polymers and Emulsion Polymerization, Ed., ACS Symp.Ser.No.165, Washington D.C.

[39] Teergarden D. M., (2004). Polymer Chemistry: Introduction to an Indispensable Science Yazar: David M. Teegarden p. 95-96

[40] Mark, J. E., Erman, B., Eirich, R., (2005). Science And Technology Of Rubber, Acedemic Press, p. 46

[41] Chern, C. S., (2008). Principles and Applications of Emulsion Polymerization pp 129, *John Wiley & Sons, Inc.,* ISBN 978-0-470-12431-4.

[42] Izumi, Z. (1967). J. Polym. Sci. Part A-1, 5: 469

[43] Morris, C. E. M., and Parts, A. G. (1976). Makromol. Chem., 177: 1433.

[44] Kozuka, K. T., Kobayashi, S., and Watanabe, A. (1973). Ger. Offen. 2,347,438 to Kanegafuchi Kagaku; C.A. (1977), 86: 30277.

[45] Kobashi, T., Shiota, H., and Umetani, H. (1977). Ger. Offen 2,709,503 to Japan Exlan; C.A. (1977), 87: 168791.

[46] O'Neill, T., and Stannett, V., (1974). J. Macromol. Sci. Chem. Part A, 8: 949.

[47] Nomura,N., (1982). Emulsion Polymerization (Piirma, I., ed.), Academic Press, NewYork, p. 191.

[48] Patsiga, R. A., Lerdthusnee, W., and Marawi, I., (1983). Org. Coat. Appl. Polym. Sci. Proc.,48: 790; C.A. (1984), 100: 157030r.

[49] Polikarpov, V. V., and Lukhovitskii, V. I., (1982). Proc. Tihany Symp. Radiat. Chem., 5: 751;C.A. (1983), 99: 140495j

[50] Ind. Chem. News (1986), 7: 10.

[51] Chem. Eng. News (1985), 27 (June 10).

[52] Norton, J. A. (1942). Chem. Rev., 31: 319.

[53] Munmaya, I., Mishra, K., Yagci, Y., (1998). Handbook of radical vinyl polymerization, p.9-11, ISBN 0-8247-9464-8

[54] Painter, P. C., and Coleman M. M., (2009). Essentials of Polymer Science and Engineering, pp 517, *DEStech Publications,Inc., ISBN* 978-1-932078-75-6

[55] Shirakawa, H., Louis, E.J., MacDiarmid, A.G., Chiang, C.K. and Heeger, A.J., (1977). *J. Chem. Soc.,Chem. Commun.*, 578.

[56] Anand, J., Palaniappan, S. And Sathyanarayan, D. N., (1998).Conductıng polyaniline blends and composites, *Prog. Polym. Sci.*, Vol. 23, 993–1018

[57] Dall'Olio, A., Dascola, Y., Varacco, V., and Bocchi, V., (1968). Acad. Sci. Ser, 267 433

[58] Gardini, C. P., (1973). Adv. Heterocyclic Chem, 15 67

[59] J.K. Avlyanov, Y. Min, A.G. MacDiarmid and A.J. Epstein, (1995). Synth. Met., 72 65 and references therein

[60] Street, G.B.; Lindsey, S.E.; Nazaal, A.I.; Wynne, K., (1985). *J. Mol. Cryst. Liq. Cryst*.,118: 137

[61] Street, G.B.; Clarke, T.C.; Geiss, R.H.; Lee, V.Y.; Nazaal, A.I.; Pfluger, P.; Scott, J.C., (1983). *J. Physique*., C3: 599

[62] Wallace G., et al., (2009). Conductive electroactive polymers: intelligent polymer systems, ISBN 978‑1‑4200‑6709‑5, p.59

[63] Ibid., p.75-77

[64] Ibid., p.79

[65] Ibid, p.80-81

[66] Li, C. M.; Sun, C. Q.; (2005). Chen, W.; Pan, L. *Surf. Coat. Technol.*, *198* (1-3), 474–477

[67] Cui, X. Q.; Li, C. M.; Zang, J. F.; Zhou, Q.; Gan, Y.; Bao, H. F.; Guo, J.; Lee, V. S.; Moochhala, S. M., (2007). *J. Phys. Chem. C*, *111*, 2025–2031.

[68] Dong, H.; Li, C. M.; Chen, W.; Zhou, Q.; Zeng, Z. X.; Luong, J. H. T., (2006). *Anal. Chem.*, *78* (21), 7424–7431.

[69] Hu, W. H.; Li, C. M.; Cui, X. Q.; Dong, H.; Zhou, Q., (2007). *Langmuir*, *23* (5), 2761–2767.

[70] Zhou, Q.; Li, C. M.; Li, J.; Cui, X. Q.; (2007).Gervasio, D. *J. Phys. Chem.C*, *111* (30), 11216–11222

[71] Diaz, A.F., Kanazawa, K.K. and Gardini, G.P., (1979). J. Chem. Soc, 635

[72] Diaz, A.F. and Hall, B.S., (1983). IBM J. Res. Develop., 27, 342

[73] Tourillon, G. And Garnier, F., J., (1982). Electroanal. Chem., , 135, 173

[74] Skotheim, T.A., Elsenbaumer, R. L., and Reynolds J. R., (1998). Handbook of conducting polymers, 2nd ed. New York: Marcel Dekker

[75] Kiebooms, R., R. Menon, and K. Lee., (2001). Synthesis, electrical, and optical properties of conjugated polymers, In Handbook of advanced electronic and photonic materials and devices, Vol. 8, ed. H.S. Nalwa. San Diego: Academic Press, pp. 1–102

[76] Pron, A., and P. Rannou., (2002). Processible conjugated polymers: From organic semiconductors to organic metals and superconductors. Prog Polym Sci 27:135–190

[77] Mitchell, G.R., F.J. Davis, and C.H. Legge., (1988). The effect of dopant molecules on the molecular order of electrically-conducting films of polypyrrole. Synth Met 26:247

[78] Bredas, J.L.; Street, G.B., (1985). *Acc. Chem. Res*., 18: 309

[79] Hu, Y.; Yang, R.; Evans, D.F.; Weaver, J.H., (1991). *Phys. Rev. B*., 44: 13660

[80] Turco, R.; Graupner, W.; Filip, C.; Bot, A.; Brie, M.; Grecu, R., (1999). *Adv. Mater. Opt. Electron*., 9: 157; and references cited therein

[81] Lee, J.Y.; Kim, D.Y.; Kim, C.Y., (1995). *Synth. Met*., 74: 103.

[82] Furukawa, Y.; Tazawa, S.; Fuji, Y.; Harada, I., (1988). *Synth. Met*., 24: 329

[83] Turco, R.; Giurgiu, L.V.; Ordean, R.; Grecu, R.; Brie, M., (2001). *Synth. Met*., 119: 287

[84] Oh, E.J.; Jang, K.S.; Suh, J.S.; Kim, H.; Kim, K.H.; Yo, C.H.; Joo, J., (1997). *Synth. Met*., 84:147

[85] Jang, K.S.; Han, S.S.; Suh, J.S.; Oh, E.J. (2001). *Synth. Met*., 119: 107

[86] Furukawa, Y., Tazawa, S., Fuji, Y., Harada, I., (1988). *Synth. Met*., 24: 329

[87] Huang, Z., Wang, P.C., Feng, J., MacDiarmid, A.G., Xia, Y., Whitesides, G.M., (1998). *Synth. Met*., 85: 1375

[88] Angelopoulos, M., (2001). Conducting polymers in microelectronics, Res. and Dev., vol. 45, no. 1

[89] Burroughes, J. H., Jones, C. A., and Friend, R. H., (1988).Nature 335, 137

[90] Tsumura, A., Koezuka, H., and Ando, T., (1988). Synth. Met. 25,11

[91] Garnier, F., Horowitz, G., Peng, X., and Fichou, D., (1990).Adv. Mater. 2, No. 12, 592

[92] Burroughes, J. H., Bradley, D., Brown, A. R., Marks, R. N., Mackey, K., Friend, R. H., Burns, P. L., and Holmes, A., (1990).Nature 347, 539

[93] G. Gustafsson, Y. Cao, G. M. Treacy, F. Klavetter, N. Colaneri, and A. J. Heeger, (1992), Nature 357, No. 11, 477

[94] Bradley, D. D. C., (1993). Synth. Met. 54, 401 and references therein

[95] Huang, Z. M.; Zhang, Y. Z.; Kotaki, M.; Ramakrishna, S., (2003)., Compos Sci Technol, 63, 2223.

[96] Ramakrishna, S.; Fujihara, K.; Teo, W. E.; Lim, T. C.; Ma, Z. (2005). In An Introduction to Electrospinning and Nanofibres; World Scientific

[97] Lee Y., S., and Sun J., (2010). Preparation of Functionalized Nanofibers and Their Applications, Nanofibers, Ashok Kumar (Ed.), ISBN: 978-953-7619-86-2

[98] Formhals A., (1934). US Patent. 1975504.Hille B. Elementary properties of ions in solution, Ion channels of excitable membranes. 3rd ed. Sunderland, Mass: Sinauer Associates, Inc.; 2001. p. 309-45

[99] Hille B., (2001). Elementary properties of ions in solution, Ion channels of excitable membranes. 3rd ed. Sunderland, Mass: Sinauer Associates, Inc.. p. 309-45

[100] Reneker, D. H.,. Yarin A. L., (2008). Electrospinning jets and polymer nanofibers, Polymer 49, 2387-2425

[101] Chew S. Y., Wen Y., Dzenis Y., Leong K. W., (2006).The role of electrospinning in the emerging field of nanomedicine. Curr Pharm Des;12:4751–70

[102] Fang, J., Niu, H., Lin, T. & Wang, X., (2008). Applications of electrospun nanofibers. *Chinese Science Bulletin,* Vol.53, No.15, pp 2265-2286

[103] Liang D, Hsiao B., S., Chu B., (2007). Functional electrospun nanofibrous scaffolds for biomedical applications. Adv Drug Deliv Rev;59:1392–412

[104] Sill T., J., Recum H. A. V., (2008) Electrospinning: applications in drug delivery and tissue enginering. Biomaterials;29:1989–2006.

[105] Huang ZM, Zhang YZ, Kotaki M, Ramakrishna S. A., (2003). Review on polymer nanofibers by electrospinning and their applications in nanocomposites. Compos Sci Technol;63:2223–53.

[106] Taylor G., I., (1969). Electrically Driven Jets. Proc R Soc Lond, A Math Phys Sci, (1934–1990), 1969; 313, 453-75

[107] Yarin A., L., Koombhongse S, Reneker D., H., (2001). Bending instability in electrospinning of nanofibers. J Appl Phys; 89:3018–26

[108] Adomaviciute E, Rimvydas M., (2007). The influence of applied voltage on poly (vinyl alcohol) (PVA) nanofibre diameter. Fibers Text East Eur;15:64–5

[109] Bhardwaj, N., Kundu, S. C., (2010). Electrospinning: A fascinating fiber fabrication technique, Biotechnology Advances 28, 325–347

[110] Chong EJ, Phan TT, Lim IJ, Zhang YZ, Bay BH, Ramakrishna S, et al., (2007). Evaluation of electrospun PCL/gelatin nanofibrous scaffold for wound healing and layered dermal reconstitution. Acta Mater;3:321–30

[111] Sukigara S., Gandhi M., Ayutsede J., Micklus M., Ko F., (2003). Regeneration of Bombyx mori silk by electrospinning—part 1:processing parameters and geometric properties. Polymer;44:5721–7

[112] Deitzel J., M., Kleinmeyer J., Harris D., Tan N., C., B., (2001). The effect of processing variables on the morphology of electrospun nanofibers and textiles. Polymer;42:261–72.

[113] Doshi J., Reneker D., H., (1995). Electrospinning process and applications of electrospun fibers. J Electrost;35:151–6.

[114] Hohman M., M., Shin M., Rutledge G., Brenner M., P., (2001). Electrospinning and electrically forced jets. II. Applications. Phys Fluids;13:2221–36.

[115] Fong H., Chun I., Reneker D., H., (1999). Beaded nanofibers formed during electrospinning.Polymer;40:4585–92

[116] Zhang C., Yuan X., Wu L., Han Y., Sheng J., (2005). Study on morphology of electrospun poly (vinyl alcohol) mats. Eur Polym J;41:423–32

[117] Pham Q., P., Sharma U., Mikos A., G., (2006). Electrospun poly (ε-caprolactone) microfiber and multilayer nanofiber/microfiber scaffolds: characterization of scaffolds and measurement of cellular infiltration. Biomacromolecules;7:2796–805

[118] Sukigara S., Gandhi M., Ayutsede J., Micklus M., Ko F., (2003) Regeneration of Bombyx mori silk by electrospinning—part 1:processing parameters and geometric properties. Polymer;44:5721–7.

[119] Ki C., S., Baek D., H., Gang K., D., Lee K., H., Um I., C., Park Y., H., (2005).Characterization of gelatin nanofiber prepared from gelatin-formic acid solution. Polymer;46:5094–102

[120] Jun Z., Hou H., Schaper A., Wendorff J., H., Greiner A., (2005) Poly-L-lactide nanofibers by electrospinning influence of solution viscosity and electrical conductivity on fiber diameter and fiber morphology. e-Polym;9:1–9.

[121] Haghi A., K., Akbari M., (2007). Trends in electrospinning of natural nanofibers. Phys Status Solidi; 204:1830–4

[122] McKee M., G., Layman J., M., Cashion M., P., (2006). Long TE. Phospholipid non-woven electrospin membranes. Science; 311:353–5

[123] Burger C., Hsiao B., S., Chu B., (2006). Nanofibrous marterials and their applications. Annu Rev Mater Res; 36:333–68.

[124] Hayati I., Bailey A., I., Tadros T., F., (1987). Investigations into the mechanisms of electrohydrodynamic spraying of liquids. 1. Effect of electric-field and the environment on pendant drops and factors affecting the formation of stable jets and atomization. J Colloid Interface Sci;117:205–21

[125] Baumgarten P., K., (1971). Electrostatic spinning of acrylic microfibers. J Colloid Interface Sci 1971;36:71–9

[126] Fong H., Reneker D., H., (1999). Elastomeric nanofibers of styrene–butadiene–styrene tri-block copolymers. J Polym Sci B Polym Phys;37:3488–93

[127] Huang L., Nagapudi K., Apkarian R., P., (2001). Chaikof EL. Engineered collagen-PEO nanofibers and fabrics. J Biomater Sci Polym Ed; 12:979–93

[128] Zong X., Kim K., Fang D., Ran S., Hsiao B., S., Chu B., (2002). Structure and process relationship of electrospun bioadsorbable nanofiber membrane. Polymer;439:4403–12

[129] Jiang H., L., Fang D., F., Hsiao B., S., Chu B., Chen W., L., (2004). Optimization and characterization of dextran membranes prepared by electrospinning. Biomacromolecules; 5: 326–33

[130] Mit-uppatham C., Nithitanakul M., Supaphol P., (2004). Ultrafine electrospun polyamide-6 fibers: effect of solution conditions on morphology and average fiber diameter. Macromol Chem Phys; 205:2327–38

[131] Zuo W., W., Zhu M., F., Yang W., Yu H., Chen Y., M., Zhang Y., (2005). Experimental study on relationship between jet instability and formation of beaded fibers during electrospinning. Polym Eng Sci; 45:704–9

[132] Kim B., Park H., Lee S., H., Sigmund W., M., (2005). Poly (acrylic acid) nanofibers by electrospinning. Mater Lett;59:829–32.

[133] Haghi A., K., Akbari M., (2007). Trends in electrospinning of natural nanofibers. Phys Status Solidi;204:1830–4

[134] Ramakrishna, S., Fujihara, K., Teo, W.E., Ma, Z.W. and Lim, T.C., (2005). An Introduction to Electrospinning and Nanofibers, *World Scientific Publishing Co. Pte. Ltd., ISBN* 981-256-415-2

[135] Taylor, G., (1964). Disintegration of Water Drops in an Electric Field, *Proc. R. Soc. Lond.,* vol.280, pp. 383-397

[136] Zhong, X. H., Kim, K. S., Fang, D. F., Ran, S. F., Hsiao, B. S. and Chu, B., (2002). Structure and process relationship of Electrospun bioabsorbable nanofiber membranes, *Polymer,* vol.43, pp. 4403-4412

[137] Deitzel, J.M., Kosik, W., McKnight, S.H., Tan, N.C.B., DeSimone, J.M. and Crette, S., (2002). Electrospinning of polymer nanofibers with specific surface chemistry, *Polymer*, vol.43, pp. 1025-1029

[138] Jarusuwannapoom, T., Hongrojjanawiwat, W., Jitjaicham, S., Wannatong, L., Nithitanakul, M., Pattamaprom, C, Koombhongse, P., Rangkupan, R. Amd Supaphol, P., (2005). Effect of solvents on electro-spinnability of polystyrene solutions and morphological appearance of resulting electrospun polystyrene fibers, *Euro. Polym. J.*, vol.41, pp. 409-421

[139] Wang, C., Hsu, C. H., and Lin, J. H., (2006). Scaling Laws in Electrospinning of Polystyrene Solutions, *Macromolecules*, vol.39, pp. 7662-7672

[140] Baker, S. C., Atkin, N., Gunning, P. A., Granville, N., Wilson, K., Wilson, D., Southgate, J., (2006). Characterisation of electrospun polystyrene scaffolds for three-dimensional in vitro biological studies, *Biomaterials*, vol.27, pp. 3136-6146

[141] Yuan X., Y., Zhang Y., Y., Dong C., H., Sheng J., (2004). Morphology of ultrafine polysulfone fibers prepared by electrospinning. Polym Int;53:1704–10.

[142] Megelski S., Stephens J., S., Chase D., B., Rabolt J., F., (2002). Micro-and nanostructured surface morphology on electrospun polymer fibers. Macromolecules;35:8456–66

[143] Zong X., Kim K., Fang D., Ran S., Hsiao B., S., Chu B., (2002). Structure and process relationship of electrospun bioadsorbable nanofiber membrane. Polymer;439:4403–12

[144] Yuan, X., Zhang, Y., Dong, C. and Sheng, J., (2004). Morphology of ultrafine polysulfone fibers prepared by electrospinning, *Polym. Int.* Vol.53, pp. 1704–10

[145] Baker, S., C., N., Atkin, P., A., (2006). Gunning, N. Granville, K. Wilson, D. Wilson, and J. Southgate, "Characterisation of electrospun polystyrene scaffolds for three-dimensional in vitro biological studies." Biomaterials 27(16):3136–3146

[146] Megelski, S., Stephens, J.S., Chase, D.B. and Rabolt, J.F., (2002). Micro- and nanostructured surface morphology on electrospun polymer fibers, *Macromolecules*, vol.35, pp. 8456-8466

[147] Jarusuwannapoom, T., Hongrojjanawiwat, W., Jitjaicham, S., Wannatong, L., Nithitanakul, M., Pattamaprom, C, Koombhongse, P., Rangkupan, R. Amd Supaphol, P., (2005). Effect of solvents on electro-spinnability of polystyrene solutions and morphological appearance of resulting electrospun polystyrene fibers, *Euro. Polym. J.*, vol.41, pp. 409-421

[148] Wang, C., Hsu, C. H., and Lin, J. H., (2006). Scaling Laws in Electrospinning of Polystyrene Solutions, *Macromolecules*, vol.39, pp. 7662-7672

[149] Wang X., Um I., C., Fang D., Okamoto A., Hsiao B., S., Chu B., (2005).Formation of water-resistant hyaluronic acid nanofibers by blowing-assisted electro-spinning and non-toxic post treatments. Polymer;46:4853–67

[150] Sundaray B., Subramanian V., Natarajan T., S., Xiang R., Z., Chang C., C., Fann W., S., (2004). Electrospinning of continuous aligned polymer fibers. Appl Phys Lett;84:1222–4

[151] Li D., Wang Y., Xia Y., (2004). Electrospinning nanofibers as uniaxially aligned arrays and layerby- layer stacked films. Adv Mater;16:361–6

[152] Xu C., Y., Inai R., Kotaki M., Ramakrishna S., (2004). Aligned biodegradable nanofibrous structure: a potential scaffold for blood vessel engineering. Biomaterials; 25:877–86

[153] Ki C., S., Kim J.,W., Hyun J., H., Lee K., H., Hattori M., Rah D., K., et al., (2007). Electrospun three dimensional silk fibroin nanofibrous scaffold. J Appl Polym Sci;106:3922–8

[154] Kumbar S., G., Nukavarapu S., P., James R., Hogan M., V., Laurencin C., T., (2008). Recent patents on electrospun biomedical nanostructures: an overview. Biomed Eng 2008;1: 68–78.

[155] Cetiner S., Kalaoglu F., Karakas H., Sarac A., S., (2010). Textile Research Journal;80:1784-1792.

[156] Yao Z., Chen H., J., Qin Y., X., Cao K., (2011). Journal of Applied Polymer Science;119:1486-1491.

[157] Vishhuvardhan, T., K., Kulkarni, V., R., Basavaraja, C., Raghavendra, S. C., (2006). Synthesis, Characterization and a.c. conductivity of polypyrrole/Y_2O_3 composites, Bull. Mater. Science, Vol. 29, No. 1, pp 77-83

[158] Cetiner, S., Karakas, H., Sarac, A. S., (2011).Dielectric, FTIR Spectroscopic and Atomic Force Microscopic Studies on Polypyrrolepoly(acrylonitrile-co-vinyl acetate) Composites, Polymer composites

[159] Cetiner, S., Sen, S., Arman, B., (2012). Acrylonitrile/Vinyl Acetate Copolymer Nanofibers with Different Vinylacetate Content, Applied polymer science(in progress)

[160] Bae W., J., Kim K., H., Jo W., H., (2005). Macromolecules;38:1044–7.]

[161] Fermin, D. J., Scharifker, B.R, J., (1993).Electroanal. Chem. 357, 273-287

[162] Cetiner, S., Kalaoglu, F., Karakas, H., Sarac., A.S., (2010). Electrospun Nanofibers of Polypyrrole-Poly(Acrylonitrile-*co*-Vinyl Acetate), Textile research journal, 2010, Vol 80(17): 1784–1792

[163] Basavaraja, C., Kim, N. R., J., et all, (2009). Transport porperties of Polypyrrole Films doped with Sulphonic Acids, Bull. Korean Chem. Soc., vol. 30, no: 11, 2701-2706

[164] Nordin, N., Ahmad, I., Daik, R., (2009).Synthesis, Characterization and thermal properties of acrylonitrile-vinyl acetate, acrylic acid terpolymer as precursor for carbon fiber, Mlaysia Polymer International Conference

[165] Brydson J., A., (1975). Plastics materials. London: Newnes-Butterworths

[166] Brent, J., L., Mulvaney, S.J., Cohen, C., Bartsch, J., A., (1997). Viscoelastic Properties of Extruded Cereal Melts. *J. Cereal Sci.*, *26*, 313–328

[167] Chronakis, I. S., Grapenson, S., and Jakob, A., (2006). Conductive Polypyrrole Nanofibers via Electrospinning: Electrical and Morphological Properties, Polymer, 47, 1597–1603.

[168] Ji, L., Yao, Y., Toprakci, O., Lin, Z., Liang, Y., Shi, Q., Medford, A J., Millns, C. R., and Zhang, X., (2010). Fabrication of Carbon Nanofiber-driven Electrodes from Electrospun Polyacrylonitrile/ Polypyrrole Bicomponents for High-performance Rechargeable Lithium-ion Batteries, *J. Power Sourc.*, 195, 2050–2056

[169] Ji, L., Medford, A. J., and Zhang, X., (2009). Electrospun Polyacrylonitrile/ Zinc Chloride Composite Nanofibers and their Response to Hydrogen Sulfide, *Polymer*, 50, 605–612

[170] Ji, L., Medford, A. J., and Zhang, X., (2009). Fabrication of Carbon Fibers with Nanoporous Morphologies from Electrospun Polyacrylonitrile/Poly(L-lactide) Blends, *J. Polymer Sci. B Polymer Phys.*, 47, 493–503 (2009).

[171] Detta, N., El-Fattah, A. A., Chiellini, E., Walkenström, P., and Gatenholm, P., (2008). Biodegradable Polymeric Micro-nanofibers byElectrospinning of Polyester/Polyether Block Copolymers, *J.Appl. Polymer Sci.*, 110, 25–261.

[172] Andrady, A. L., (2008).“Science and Technology of Polymer Nanofibers”, John Wiley & Sons, Inc., New Jersey, USA

[173] Han N, Zhang X., X., Wang X., C, W., N., (2010). Macromolecular Research;18:144-152.

CURRICULUM VITAE

Name Surname: Burcu Arman

Place and date of birth: Balıkesir- 26.05.1986

Address: Şair Arşi caddesi, Hamle Sok. Kutlu apt., No:18, Göztepe-Kadıköy/ İSTANBUL

E-mail: brc_arman@hotmail.com

B.Sc.: Istanbul Technical University- Textile Engineering (2010)

M.Sc.: Istanbul Technical University- Polymer Science and Technology (2012)

PUBLICATIONS/PRESENTATIONS ON THE THESIS

- **ARMAN, B., SARAC, A.S.,** 2012: Electrospun nanofibers of Poly(Acrylonitrile-co-Vinyl Acetate)/Polypyrrole composites, *POLYCHAR 20 World Forum on Advanced Materials,* March 26-30,2012 Dubrovnik,CROATIA.